



1 Unbalanced emission reductions of different species and sectors in 2 China during COVID-19 lockdown derived by multi-species surface 3 observation assimilation

4 Lei Kong^{1,3}, Xiao Tang^{*,1,3}, Jiang Zhu^{2,3}, Zifa Wang^{1,3,4}, Yele Sun^{1,3}, Pingqing Fu⁵, Meng Gao⁶,
5 Huangjian Wu^{1,3}, Miaomiao Lu⁷, Qian Wu^{1,3}, Shuyuan Huang⁸, Wenxuan Sui¹, Jie Li^{1,3}, Xiaole Pan^{1,3},
6 Lin Wu^{1,3}, Hajime Akimoto⁹, Gregory R. Carmichael¹⁰

7 ¹State Key Laboratory of Atmospheric Boundary Layer Physics and Atmospheric Chemistry (LAPC), Institute of
8 Atmospheric Physics, Chinese Academy of Sciences, Beijing 100029, China

9 ²CAS-TWAS Center of Excellence for Climate and Environment Sciences (ICCES), Institute of Atmospheric Physics,
10 Chinese Academy of Sciences, Beijing 100029, China

11 ³University of Chinese Academy of Sciences, Beijing 100049, China

12 ⁴Center for Excellence in Regional Atmospheric Environment, Institute of Urban Environment, Chinese Academy of
13 Sciences, Xiamen 361021, China

14 ⁵Institute of Surface-Earth System Science, Tianjin University, Tianjin 300072, China

15 ⁶Department of Geography, State Key Laboratory of Environmental and Biological Analysis, Hong Kong Baptist University,
16 Hong Kong SAR, China

17 ⁷State Environmental Protection Key Laboratory of Urban Ambient Air Particulate Matter Pollution Prevention and Control,
18 College of Environmental Science and Engineering, Nankai University, Tianjin 300350, China

19 ⁸Chengdu University of Information Technology, Chengdu 610225, China

20 ⁹National Institute for Environmental Studies, Onogawa, Tsukuba 305-8506, Japan

21 ¹⁰Center for Global and Regional Environmental Research, University of Iowa, Iowa City, IA 52242, USA

22 *Correspondence to:* Xiao Tang (tangxiao@mail.iap.ac.cn)

23 **Abstract.** The unprecedented lockdown of human activities during the COVID-19 pandemic have significantly influenced
24 the social life in China. However, understanding of the impact of this unique event on the emissions of different species is
25 still insufficient, prohibiting the proper assessment of the environmental impacts of COVID-19 restrictions. Here we
26 developed a multi-air pollutant inversion system to simultaneously estimate the emissions of NO_x, SO₂, CO, PM_{2.5} and PM₁₀
27 in China during COVID-19 restrictions with high temporal (daily) and horizontal (15km) resolutions. Subsequently,
28 contributions of emission changes versus meteorology variations during COVID-19 lockdown were separated and quantified.
29 The results demonstrated that the inversion system effectively reproduced the actual emission variations of multi-air
30 pollutants in China during different periods of COVID-19 lockdown, which indicate that the lockdown is largely a
31 nationwide road traffic control measurement with NO_x emissions decreased substantially by ~40%. However, emissions of
32 other air pollutants were found only decreased by ~10%, both because power generation and heavy industrial processes were
33 not halted during lockdown, and residential activities may actually have increased due to the stay-at-home orders.
34 Consequently, although obvious reductions of PM_{2.5} concentrations occurred over North China Plain (NCP) during
35 lockdown period, the emission change only accounted for 8.6% of PM_{2.5} reductions, and even led to substantial increases of
36 O₃. The meteorological variation instead dominated the changes in PM_{2.5} concentrations over NCP, which contributed 90%



37 of the $PM_{2.5}$ reductions over most parts of NCP region. Meanwhile, our results also suggest that the local stagnant
38 meteorological conditions together with inefficient reductions in $PM_{2.5}$ emissions were the main drivers of the unexpected
39 COVID-19 haze in Beijing. These results highlighted that traffic control as a separate pollution control measure has limited
40 effects on the coordinated control of O_3 and $PM_{2.5}$ concentrations under current complex air pollution conditions in China.
41 More comprehensive and balanced regulations for multiple precursors from different sectors are required to address O_3 and
42 $PM_{2.5}$ pollution in China.

43 **1 Introduction**

44 A novel coronavirus disease (COVID-19) broke out in Wuhan at the end of 2019 but quickly spread across the whole
45 China within a month. To curb the spread of the virus, strict epidemic control measures were implemented by Chinese
46 governments to prevent large gatherings, including strict travel restriction, shutting down of non-essential industries,
47 extended holidays, closing of schools and entertainment houses (Cheng et al., 2020). These restrictions have had a significant
48 impact on the industrial activities and social life, as exemplified by the drop of China's industrial output by 15-30%
49 (<https://data.stats.gov.cn/>, last accessed on 22 Oct, 2022) and the dramatic decrease of traffic flow by 60–90% in major cities
50 of China during COVID-19 epidemic (<http://jiaotong.baidu.com/>, last accessed on 22 Oct, 2022), which provides us a natural
51 experiment to examine the responses of the emissions and air quality on the changes in human activities.

52 It has been well documented that the short-term stringent emission control targeted on power generator or heavy
53 industry enacted by Chinese government during certain societal events, such as the 2008 Olympics Games, 2014 Asia-
54 Pacific Economic Cooperation conference and 2015 China Victory Day Parade, is an effective way to reduce emissions and
55 improve air quality (Okuda et al., 2011; Wang et al., 2014; Tang et al., 2015; Zhang et al., 2016; Wu et al., 2020; Chu et al.,
56 2018). However, different from those stringent emission controls, the COVID-19 restrictions are inclined to affect emissions
57 from sectors more closely to social life whose influence on emissions has still not well been assessed. Previous studies
58 suggest that the COVID-19 restrictions have substantially reduced the China's anthropogenic emissions from almost all
59 sectors (Zheng et al., 2021; Huang et al., 2021; Xing et al., 2020). For example, by using a bottom-up method based on near-
60 real-time activity data, Zheng et al. (2021) reported that the emissions of NO_x , SO_2 , CO and primary $PM_{2.5}$ decreased by 36%,
61 27%, 28% and 24% during COVID-19 restrictions, mostly due to the reductions in industry and transportation sector. Xing
62 et al. (2020), by using a response model, estimated stronger COVID-19 shutdown effects on emissions over the North China
63 Plain (NCP) with emissions of NO_x , SO_2 and primary $PM_{2.5}$ dropped by 51%, 28% and 63%, respectively. Others argue that
64 the COVID-19 restriction may mainly affect the emissions from transportation, light industry and manufacturing, while it
65 has much smaller effects on the emissions from the power generator and heavy industry because of their non-interruptible
66 processes (Chu et al., 2021; Hammer et al., 2021; Le et al., 2020; Zhao et al., 2020). Moreover, the residential emissions may
67 even increase during the COVID-19 lockdown due to the increased demanding for space heating and cooking with the stay-
68 at-home orders. Therefore, Le et al. (2020) only considered the NO_x reductions during COVID-19 restrictions in their



69 investigation of the severe haze during COVID-19 lockdown, and similarly, Hammer et al. (2021) only considered the
70 emission reductions in the transportation sector. This indicates that there has large uncertainty in the current understanding of
71 the effects of COVID-19 restrictions on the emissions of different species.

72 Quantification of the emission changes of different species and different sectors during the COVID-19 lockdown is thus
73 necessary for the comprehensive understanding of the environmental impacts of COVID-19 restrictions. In particular,
74 although observations indeed show decreases of air pollutant concentrations during COVID-19 restrictions (Fan et al., 2020;
75 Wang et al., 2021; He et al., 2020; Shi and Brasseur, 2020), the air quality improvement is much smaller than the expected
76 (Shi et al., 2021; Diamond and Wood, 2020; Yan et al., 2022). Moreover, severe haze (COVID-19 haze) still occurred in
77 northern China (Sulaymon et al., 2021; Le et al., 2020) and O₃ concentrations even showed significant increases (Zhang et
78 al., 2021; Li et al., 2020). A number of studies were conducted to explain this air quality change by analyzing the effects of
79 emission changes, meteorological variations and secondary production (Huang et al., 2021; Le et al., 2020; Hammer et al.,
80 2021; Zhao et al., 2020; Zhao et al., 2021; Sulaymon et al., 2021; Wang et al., 2020; Li et al., 2021). However, due to the
81 unknown emission changes during COVID-19 restrictions, the emission reduction scenarios that used to represent the
82 COVID-19 shutdown effects varied among different studies and did not consider the spatial and temporal heterogeneity of
83 the emission changes, leading to biases in the model simulation (Zhao et al., 2021; Li et al., 2021; Hammer et al., 2021;
84 Zheng et al., 2021) and uncertainty in the quantification of the contributions of different factors.

85 Pioneer studies by Zheng et al. (2021) and Forster et al. (2020) have derived multi-air pollutant emissions from social
86 activity data using a bottom-up method, but due to the lack of detailed social activity data, large uncertainties existed in their
87 estimates. The meteorologically and seasonally driven variability of the concentrations of air pollutants also prohibit drawing
88 fully quantitative conclusions on the changes of emissions based on observations alone (Levelt et al., 2022). The emission
89 inversion technique, which takes advantage of the chemical transport model (CTM) and real-time observations, provides an
90 attractive way to estimate the sector-specific and space-based emission changes during COVID-19 restrictions (Levelt et al.,
91 2022), as shown in Zhang et al. (2020), Zhang et al. (2021), Feng et al. (2020) and Hu et al. (2022). However, these studies
92 only inversed the emissions of single species (e.g., NO_x and SO₂) without insights into multiple species. In view of this
93 discrepancy, in this study we developed a multi-air pollutant inversion system to simultaneously estimated the multi-air
94 pollutant emissions in China, including NO_x, SO₂, CO, PM_{2.5} and PM₁₀, during the COVID-19 restrictions using an ensemble
95 Kalman filter (EnKF) and surface observations from the China National Environmental Monitoring Centre (CNEMC).
96 Subsequently, the inversed emission inventory was used to quantify the contributions of emission changes versus
97 meteorology variations to the changes in PM_{2.5} and O₃ concentrations over the NCP region during the COVID-19 restrictions.

98 **2 Method and data**

99 We developed a high-resolution multi-air pollutant inversion system to estimate the daily emissions of NO_x, SO₂, CO,
100 PM_{2.5} and PM₁₀ in China during the COVID-19 restrictions. This system uses the NAQPMS (Nested Air Quality Prediction



101 Modelling System) model as the forecast model and the EnKF coupled with the state argumentation method as the inversion
102 method. It has the capabilities of simultaneous inversion of multi-air pollutant emissions at high temporal (daily) and spatial
103 (15km) resolutions. An iteration inversion scheme was also developed in this study to address the large biases in the a priori
104 emissions. In the following sections, we briefly introduce each component of the inversion system.

105 2.1 Chemical transport model and its configuration

106 The NAQPMS model was used as the forecast model to represent the atmospheric chemistry in this study, which has
107 been used in previous inversion studies (Tang et al., 2011; Tang et al., 2013; Kong et al., 2019; Wu et al., 2020), where
108 detailed descriptions of NAQPMS are available. The Weather Research and Forecasting Model (WRF)(Skamarock, 2008) is
109 used to provide the meteorological inputs to the NAQPMS model.

110 Figure 1 shows the modelling domain of this study with a high horizontal resolution of 15 km. The a priori emission
111 inventory used in this study includes monthly anthropogenic emissions from the HTAP_v2.2 emission inventory for the base
112 year of 2010 (Janssens-Maenhout et al., 2015), biomass burning emissions from the Global Fire Emissions Data base (GFED)
113 version 4 (Randerson et al., 2017; Van Der Werf et al., 2010), biogenic volatile organic compound (BVOC) emissions from
114 MEGAN-MACC (Sindelarova et al., 2014), marine volatile organic compound emissions from the POET database (Granier
115 et al., 2005), soil NO_x emissions from the Regional Emission inventory in Asia (Yan et al., 2003) and lightning NO_x
116 emissions from Price et al. (1997). Chemical top and boundary conditions were provided by the global CTM MOZART
117 (Model for Ozone and Related Chemical Tracers) (Brasseur et al., 1998; Hauglustaine et al., 1998). We assumed no monthly
118 variations in the a priori emission inventory and used January's emission inventory for the whole simulation period so that
119 the emission variation was solely derived from the surface observations. A two-week free run of NAQPMS was conducted
120 as a spin-up time. For each day's meteorological simulation, a 36-h free run of WRF was conducted, of which the first 12-h
121 simulation was a spin-up run and the next 24-h simulation provided the meteorological inputs to NAQPMS. Initial and
122 boundary conditions for the meteorological simulation were provided by the National Center for Atmospheric
123 Research/National Center for Environment Prediction (NCAR/NCEP) 1° × 1° reanalysis data. Evaluation results for the
124 WRF simulation are available in Text S1 in Supplement.

125 2.2 Surface Observations

126 The hourly concentrations of NO₂, SO₂, CO, PM_{2.5} and PM₁₀ from CNEMC were used in this study to estimate the
127 emissions during COVID-19. The spatial distributions of these observation sites are shown in Fig. 1, which contains 1436
128 observation sites covering most regions of China. Before assimilation, outliers of observations were first filtered out using
129 the automatic outlier detection method developed by Wu et al. (2018) to prevent the adverse effects of the outliers on data
130 assimilation. Then, the hourly concentrations were averaged to the daily values for the inversions of daily emissions.

131 The observation error is one of the key inputs to the data assimilation, which together with the background error
132 determine the relative weights of the observation and background values on the analysis. The observation error includes



133 measurement error and representativeness error. The measurement error of each species was designated according to the
134 officially released documents of the Chinese Ministry of Ecology and Environmental Protection (HJ 193-2013 and HJ 654-
135 2013, available at <http://www.cnemc.cn/jcggf/dqjh/>, last accessed on 22 Oct 2022), which is 5% for PM_{2.5} and PM₁₀ and 2%
136 for SO₂, NO₂ and CO. A representativeness error arises from the different spatial scales that the discrete observation data and
137 model simulation represent, which was estimated based on the previous study by Li et al. (2019) and Kong et al. (2021).

138 2.3 Inversion estimation scheme

139 The EnKF coupled with the state augmentation method was used in this study to constrain the emissions of multiple
140 species. EnKF is an advanced data assimilation method proposed by Evensen (1994) that features representation of the
141 uncertainties of the model state by a stochastic ensemble of model realizations. It is easily implemented and can update the
142 state variable by using the flow-dependent background error covariance matrix. In the state augmentation method, the
143 emissions of different species, together with the concentrations of related species, were treated as the state variable and were
144 updated according to the relationship between the emissions and concentrations of related species.

145 Since the source emission data over mainland China in HTAP_v2.2 inventory is obtained from the MIX inventory (Li et
146 al., 2017b), uncertainties of emissions of different species, including PMF, PMC, BC, OC, NO_x, CO, SO₂, NH₃ and NMVOC
147 (nonmethane volatile organic compounds), were obtained from Li et al. (2017b) and Streets et al. (2003), which were
148 represented by an ensemble of perturbed emissions generated by multiplying the a priori emissions with a perturbation factor
149 $\beta_{i,s}$:

$$150 \mathbf{E}_{i,s} = \beta_{i,s} \circ \mathbf{E}_s^p, \quad i = 1, 2, \dots, N_{ens} \quad (1)$$

151 where $E_{i,s}$ represents the vector of the i th member of perturbed emissions for species s , E_s^p represents the a priori emissions
152 for this species, \circ denotes the schur product and N_{ens} denotes the ensemble size. Thus, the adjustment of emissions is
153 equivalent to the adjustment of perturbation factors.

154 Considering that emission uncertainty is the major contributor to the uncertainties in air quality modelling, especially
155 during the COVID-19 period when emissions changed rapidly, uncertainties in chemical variables were obtained through
156 ensemble simulations driven by perturbed emissions. The ensemble size was chosen as 50 to maintain the balance between
157 the filter performance and computational cost. After the ensemble simulations, emissions of multiple species were updated
158 using a deterministic form of EnKF (DEnKF) proposed by Sakov and Oke (2008), which is formulated by

$$159 \bar{\mathbf{x}}^a = \bar{\mathbf{x}}^b + \mathbf{P}_e^b \mathbf{H}^T (\mathbf{H} \mathbf{P}_e^b \mathbf{H}^T + \mathbf{R})^{-1} (\mathbf{y}^o - \mathbf{H} \bar{\mathbf{x}}^b) \quad (2)$$

$$160 \bar{\mathbf{x}}^b = \frac{1}{N} \sum_{i=1}^N \mathbf{x}_i^b; \quad \mathbf{X}_i^b = \mathbf{x}_i^b - \bar{\mathbf{x}}^b \quad (3)$$

$$161 \mathbf{P}_e^b = \frac{1}{N-1} \sum_{i=1}^N \mathbf{X}_i^b (\mathbf{X}_i^b)^T \quad (4)$$

162 where \mathbf{x} denotes the state variables; b the background state (a priori); a the analysis state (posteriori); \mathbf{P}_e^b the ensemble-
163 estimated background error covariance matrix and N the ensemble size. \mathbf{y}^o represents the vector of observations with an



164 error covariance matrix of \mathbf{R} . \mathbf{H} is the linear observational operator that maps the m -dimensional state vector \mathbf{x} to a p -
165 (number of observations) dimensional observational vector ($\mathbf{H}\mathbf{x}^b$). The state variables were defined as follows according to
166 state augmentation method during the assimilation:

$$167 \mathbf{x}_i = [\mathbf{c}_i, \boldsymbol{\beta}_i]^T, i = 1, 2, \dots, N_{ens} \quad (5)$$

$$168 \mathbf{c}_i = [PM_{2.5}, PM_{10-2.5}, NO_2, SO_2, CO]_i \quad (6)$$

$$169 \boldsymbol{\beta}_i = [\beta_{PMF}, \beta_{BC}, \beta_{OC}, \beta_{PMC}, \beta_{NO_x}, \beta_{SO_2}, \beta_{CO}]_i \quad (7)$$

170 where \mathbf{x}_i represents the i th member of the assimilated state variable, which consists of the fields of chemical variables \mathbf{c}_i
171 and emission perturbation factors $\boldsymbol{\beta}_i$. Detailed descriptions of the model state variables are summarized in Table 1. The use
172 of $PM_{10-2.5}$ (PM_{10} minus $PM_{2.5}$) values aims to avoid the potential cross-correlations between $PM_{2.5}$ and PM_{10} (Peng et al.,
173 2018; Ma et al., 2019). Moreover, to prevent spurious correlations between non- or weakly related variables, similar to Ma et
174 al. (2019) and Miyazaki et al. (2012), state variable localization was used during assimilation, with observations of one
175 particular species only allowing us to update the emissions of the same species. The corresponding relationship between the
176 chemical observations and adjusted emissions is summarized in Table 1. The $PM_{2.5}$ observations were one exception and
177 were used to update the emissions of PMF (fine mode unspciated aerosol), BC (black carbon) and OC (organic carbon)
178 since the observations of speciated $PM_{2.5}$ were not available in this study. The lack of speciated $PM_{2.5}$ observations may lead
179 to uncertainties in the estimated emissions of PMF, BC and OC. Therefore, we only analyzed the emissions of $PM_{2.5}$, which
180 were the sum of the emissions of these three species. Similarly, only PM_{10} emissions were analyzed in this study, which
181 includes the emissions of $PM_{2.5}$ and PMC (coarse mode unspciated aerosol).

182 Due to the strict control measures implemented during the last decades, the emissions in China decreased dramatically
183 from 2010 to 2020, especially for SO_2 . Thus, there are large biases in the a priori estimates of emissions in China (Zheng et
184 al., 2018), which would lead to incomplete adjustments of a priori emissions and degrade the performance of assimilation.
185 Therefore, an iteration inversion scheme was developed in this study to address the large biases of SO_2 emissions. As
186 illustrated in Fig. 2, the main idea of the iteration inversion scheme is to update the ensemble mean of the state variable using
187 the inversion results of the k th iteration and corresponding simulations. The state variable used in the $(k + 1)$ th inversions
188 is written as follows:

$$189 \mathbf{x}_i^{k+1} = [\mathbf{c}^k + \mathbf{c}_i^e - \bar{\mathbf{c}}^e, \boldsymbol{\beta}^k + \boldsymbol{\beta}_i^e - \bar{\boldsymbol{\beta}}^e]^T \quad (8)$$

190 where \mathbf{c}^k represents the simulation results using the inversed emissions of the k th iteration, \mathbf{c}_i^e represents the i th member of
191 ensemble simulations with an ensemble mean of $\bar{\mathbf{c}}^e$, $\boldsymbol{\beta}^k$ represents the perturbation factors of the k th iteration, and
192 $\boldsymbol{\beta}_i^e$ represents the i th member of the ensemble of perturbation factors with a mean value of $\bar{\boldsymbol{\beta}}^e$.

193 Using this method, the biases of a priori emissions were well addressed as exemplified in Fig. 3 for SO_2 emissions. Due
194 to the large positive biases in the a priori SO_2 emissions, the model still has large positive biases (NMB = 30.9–220.5%) and
195 errors (RMSE = 8.7–23.0 $\mu\text{g}/\text{m}^3$) in simulating SO_2 concentration over all regions of China even after the assimilation (first
196 iteration). The biases and errors continued to decrease with the increasing of iteration times till the fourth iteration in which



197 there were no significant improvement in SO₂ simulations compared to those in third iteration. These results suggested that
198 the iteration inversion method used in this study can well constrain the a priori emission with large biases and, in this
199 application, conducting three iteration is enough for constraining the emission. Besides SO₂ emissions, the iteration inversion
200 scheme was also applied to the emissions of other species.

201 To reduce the influences of random model errors (e.g., errors in meteorological inputs) on the estimation of the
202 variation in emissions, a 15-day running average was performed on our daily inversion results after the inversion estimation.
203 It should be noted that the COVID-19 restrictions were initiated during the Spring Festival of China, which would also
204 influence the air pollutant emissions in China. However, the inversion method used in this study did not differentiate the
205 contributions of the Spring Festival from the COVID-19 restrictions. Similarly, the effects of natural emission changes were
206 not differentiated in this study, which would lead to uncertainty in quantifying the effects of the COVID-19 restrictions on
207 air pollutant emissions.

208 **2.4 Quantification of the effects of emission changes and meteorological variations**

209 In previous studies, the meteorological-induced (MI) changes were usually determined by the CTM with a fixed
210 emission input setting and a varying meteorological input. Then, the difference between the MI changes and total changes in
211 air pollutant concentrations is defined as emission-induced (EI) changes. Another approach to estimate EI changes is to
212 perform simulations with a fixed meteorological input setting and varying emission inputs. Then, the MI changes are defined
213 as the difference between EI changes and total changes in air pollutant concentrations. Due to the nonlinear effects of
214 atmospheric chemical systems, these two methods yield different results. Thus, both methods were used in this study to
215 account for the nonlinear effects. The averaged results of these two methods are used to represent the impacts of emission
216 changes and meteorological variation on the air quality changes during the COVID-19 restrictions. In total, three scenario
217 experiments were designed based on our inversion results. The first scenario simulation used the varying meteorological and
218 emission inputs from the P1 to P2 period, which represents the real-world scenario and is used to estimate the total changes
219 in air pollutant concentrations induced by emissions and meteorological changes from the P1 to P2 period (BASE scenario).
220 The second scenario experiment used the varying meteorological inputs but replaced the emissions during the P2 period with
221 those during the P1 period, which was used to estimate the MI changes using the first method (MET change scenario). The
222 third scenario experiment used the varying emissions input and replaced the meteorological input during the P2 period with
223 that during the P1 period, which was used to estimate the EI changes using the second method (EMIS change scenario).
224 Based on the first method, the MI and EI changes can be estimated as follows:

$$225 \quad MI_{MET \text{ change scenario}} = conc_{p2, MET \text{ change scenario}} - conc_{p1, MET \text{ change scenario}} \quad (9)$$

$$226 \quad EI_{MET \text{ change scenario}} = conc_{p2, BASE \text{ scenario}} - conc_{p1, BASE \text{ scenario}} - MI_{MET \text{ change scenario}} \quad (10)$$

227 where $MI_{MET \text{ change scenario}}$ represents the MI changes estimated based on the results from the MET change scenario,
228 $conc_{p1, MET \text{ change scenario}}$ and $conc_{p2, MET \text{ change scenario}}$ represent the averaged concentrations of air pollutants during the



229 P1 and P2 periods under the MET change scenario, $EI_{MET\ change\ scenario}$ represents the EI changes estimated based on the
230 results from the MET change scenario, and $conc_{p1,BASE\ scenario}$, $conc_{p2,BASE\ scenario}$ respectively represent the averaged
231 concentrations of air pollutants during the P1 and P2 periods under the BASE scenario. Similarly, the MI and EI changes
232 estimated based on the second method are formulated as follows:

$$233\ EI_{EMIS\ change\ scenario} = conc_{p2,EMIS\ change\ scenario} - conc_{p1,EMIS\ change\ scenario} \quad (11)$$

$$234\ MI_{EMIS\ change\ scenario} = conc_{p2,BASE\ scenario} - conc_{p1,BASE\ scenario} - EI_{EMIS\ change\ scenario} \quad (12)$$

235 Then, the estimations from these two methods are averaged to estimate the contributions of meteorological change and
236 emission change to the changes in $PM_{2.5}$ and O_3 concentrations during the COVID-19 lockdown:

$$237\ MI = (MI_{EMIS\ change\ scenario} + MI_{MET\ change\ scenario})/2 \quad (13)$$

$$238\ EI = (EI_{EMIS\ change\ scenario} + EI_{MET\ change\ scenario})/2 \quad (14)$$

$$239\ contri_{met} = \frac{MI}{MI+EI} \times 100 \quad (15)$$

$$240\ contri_{emis} = \frac{EI}{MI+EI} \times 100 \quad (16)$$

241 where $contri_{met}$ and $contri_{emis}$ represent the relative contributions (%) of the meteorological variations and emission
242 changes to the changes in air pollutant concentrations.

243 3 Results

244 We estimated the multi-air pollutant emissions from 1 Jan to 29 Feb 2020 when the pandemic was at its most serious,
245 and the effects of the COVID-19 restrictions were most profound in China. According to different control phases of COVID-
246 19 and the timing of the Chinese Lunar New Year, the whole time period was divided into three periods: before lockdown
247 (P1, January 1-20), lockdown (P2, January 21-February 9) and after back-to-work day (P3, February 10-29) to better
248 characterize the emission changes during the COVID-19 restrictions. Additionally, we analyzed the emission changes in
249 different regions of China, including the North China Plain (NCP), Northeast China (NE), Southeast China (SE), Southwest
250 China (SW), Northwest China (NW) and Central regions (defined in Fig. 1) to investigate the responses of emissions to the
251 COVID-19 restrictions in different regions.

252 3.1 Validation of the inversion results

253 We firstly validate our inversion system by using a cross-validation, in which 20% of observation sites were withheld
254 from the emission inversion and used as the validation datasets. Figure S1–6 showed the concentrations of different air
255 pollutants in China from 1st Jan to 29th Feb 2020 obtained from observations at validation sites and simulations using a priori
256 and a posteriori emission. Commonly used statistical evaluation indices, including correlation coefficient (R), mean bias
257 error (MBE), normalized mean bias (NMB) and root of mean square error (RMSE) are summarized in Table S1. The
258 validation results suggest that the posteriori simulation agreed well with the observed concentrations for all species. The



259 large biases in the a priori simulation of $PM_{2.5}$, PM_{10} , SO_2 and CO were almost completely removed in the a posteriori
260 simulation with NMB about -3.9–15.7% for $PM_{2.5}$, -3.1–11.6% for PM_{10} , -12.6–5.3% for NO_2 , -9.5–6.2% for SO_2 and -10–
261 7.6% for CO (Table S4). RMSE values were also significantly reduced in the a posteriori simulation which were 9.1–
262 $32.2\mu\text{g}/\text{m}^3$ for $PM_{2.5}$, $12.6\text{--}42.4\mu\text{g}/\text{m}^3$ for PM_{10} , $5.1\text{--}12.3\mu\text{g}/\text{m}^3$ for NO_2 , $1.2\text{--}5.6\mu\text{g}/\text{m}^3$ for SO_2 and $0.10\text{--}0.46\text{mg}/\text{m}^3$ for
263 CO. Moreover, the inversion emission considerably improved the fit to the observed time evolution of air pollutants'
264 concentrations. The R values were improved for all species in the a posteriori simulation that were up to 0.74–0.94 for $PM_{2.5}$,
265 0.63 – 0.92 for PM_{10} , 0.76–0.94 for NO_2 , 0.23–0.79 for SO_2 and 0.63–0.92 for CO. These results suggest that our inversion
266 results have excellent performance in representing the magnitude and variation of these species' emission in China during
267 COVID-19 restrictions. Model performance in simulating O_3 concentration is relatively poor compared to other species
268 although improvement was remarkable in NCP, NE and SE regions. This would be due to that the emission of volatile
269 organic compounds, another important precursor for O_3 , were not constrained in this study.

270 **3.2 Emission changes of multi-species during COVID-19 restrictions**

271 **3.2.1 Unbalanced emission changes between NO_x and other species**

272 The control of COVID-19 began on 23rd January when the Chinese government declared the first level of national
273 responses to public health emergencies, one day before the 2020 Chinese New Year Eve. Figure 4 shows the time evolution
274 of the normalized emission anomaly for different species in China from 1st January to 29th February. The temporal variation
275 in the emission varied largely between NO_x and other species. Due to the combined effects of the Spring Festival and
276 COVID-19 lockdown, NO_x emissions decreased continuously at the beginning of January until approximately one week after
277 the implementation of the COVID-19 lockdown, with estimated decreases in NO_x emissions of up to 46.7% from the P1 to
278 P2 period (Table 2). Subsequently, the NO_x emissions stabilized with small fluctuations until the official back-to-work day
279 when the NO_x emissions began to increase due to easing of the control measures and the resumption of business. According
280 to inversion estimation, NO_x emissions recovered by 6.5% during the P3 period. These results indicate that the temporal
281 variation in our estimated NO_x emissions agreed well with the timing of the Spring Festival and different control stages of
282 COVID-19. However, for other species (i.e., $PM_{2.5}$, PM_{10} , SO_2 and CO), although their emissions generally decreased from
283 1st January to the end of the 2020 Spring Festival holiday, they showed much smaller reductions than the NO_x emissions.
284 The emission reduction for these species was only approximately 7.9-12.1% (Table 2). This is consistent with the inversion
285 results by Hu et al. (2022) who found that SO_2 emissions in China decreased only by 9.2% during COVID-19 lockdown. In
286 addition, the emissions of these species quickly rebounded to their normal level just one week after the end of the Spring
287 Festival holiday. As estimated by our inversion results, the SO_2 emissions recovered by 7.2% during the P3 period, which
288 was only 2.5% lower than that during the P1 period. The $PM_{2.5}$ and PM_{10} emissions during the P3 period were 3.3% and 43.6%
289 higher, respectively, than those during the P1 period.



290 Similar results were found in different regions of China (Fig. 5 and Table 3), where the NO_x emissions decreased much
291 more than other species. In addition, unlike the uniform decreases in NO_x emissions in different regions of China (~45%),
292 there was apparent spatial heterogeneity in the emission changes in $\text{PM}_{2.5}$, PM_{10} , SO_2 and CO (Table 3 and Fig. 6). For
293 example, from the P1 to P2 period, the $\text{PM}_{2.5}$ emissions decreased by over 20% in the Central region but only by 8.8% in the
294 NE region. The $\text{PM}_{2.5}$ emissions even increased by 5.5% in the NCP region, possible due to the increased emissions from
295 heating and fireworks (Dai et al., 2020). The SW and central regions exhibited relatively larger emission reductions for these
296 species (Fig. 5 and Table 3) by 12.6–25.9% and 10.6–23.7%, respectively. The emission rebound during the P3 period was
297 more prominent in the SE, central and SW regions (Fig. 5 and Fig. 7), where emissions recovered by 6.0–16.4% for NO_x ,
298 7.5–19.8% for SO_2 , 7.4–13.1% for CO, 12.3–47.7% for $\text{PM}_{2.5}$ and 28.6–135.9% for PM_{10} (Table 3). This result is consistent
299 with the earlier degradation of the response level to the COVID-19 virus (from the first level to the second or third level)
300 over these regions (Table S2). In contrast, there were decreases in emissions in the NCP, NE and NW regions. $\text{PM}_{2.5}$
301 emissions were reduced by 9.9% in the NCP region and by 19.2% in the NE region from the P2 to P3 period (Table 3).
302 Moreover, we found that the PM_{10} emissions surged in the NW and central regions, where the PM_{10} emissions during the P3
303 period were almost two times larger than those during the P2 period (Table 3). However, this finding may be related to the
304 enhanced sandstorms over these two regions rather than the effects of returning to work, which demonstrates the necessity to
305 consider changes in natural emissions during COVID-19 restrictions. Thus, to reduce the effects of natural emissions on our
306 findings, the same analysis was performed for the emissions over east China (Fig. S7) where emissions were dominated by
307 anthropogenic sources, which shows consistent results with the findings above (Fig. S8 and Table S3).

308 3.2.3 Explanations for the emission changes during COVID-19 restrictions

309 Two explanations may help clarify the unbalanced emission changes between NO_x and other species. First, the COVID-
310 19 lockdown policy has led to dramatic decreases in transportation activities throughout China; however, as shown in Fig. 4,
311 the relative contributions of the transportation sector to the emissions of SO_2 (2.4%), CO (18.5%), $\text{PM}_{2.5}$ (6.1%) and PM_{10}
312 (4.7%) are much smaller than those for NO_x emissions (34.3%) (Zheng et al., 2018; Li et al., 2017a). Thus, the reduction in
313 traffic activities can only substantially decrease NO_x emissions. Reductions in CO emissions were relatively larger than those
314 for SO_2 and $\text{PM}_{2.5}$ emissions, which is consistent with the relatively larger contributions of the transportation sector to CO
315 emissions. PM_{10} emissions showed the largest reductions among these four species, which is related in part to the reduced
316 dust emissions due to shutting down of construction sites during the lockdown period (Li et al., 2020). Second, as shown in
317 Fig. 4, the industrial and residential sectors are the major contributors to the anthropogenic emissions of SO_2 , CO, $\text{PM}_{2.5}$ and
318 PM_{10} in China, together contributing 77.6%, 78.3%, 86.5% and 86.3%, respectively, to their total emissions. The much
319 smaller reductions of these species' emissions were thus in line with the fact that there were no intentional restrictions on
320 heavy industry during the COVID-19 restrictions. A large number of non-interruptible processes, such as steel, glass, coke,
321 refractory, petrochemical, electric power, and especially heating, cannot be stopped during the COVID-19 lockdown.
322 According to statistical data from the National Bureau of Statistics of China (Fig. S9), the industrial and power sectors did



323 not show similar reductions in their activity levels as those seen in the transportation sector. Power generation and steel
324 production even showed increases in many provinces, which corresponds well with the emission increases over these regions.
325 In addition, since people were required to stay at home, residential emissions were likely increased due to the increased
326 energy consumption for heating or cooking. Therefore, our inversion results supported the views that the emissions of
327 species related to industrial and residential activities did not decline much during the lockdown period, and that the COVID-
328 19 lockdown policy was largely a traffic control measure with small influences on other sectors.

329 **3.3 Investigation of air quality change over the NCP region during COVID-19 restrictions**

330 Using the inversion results, we reassessed the environmental impacts of the COVID-19 restrictions on the air pollution
331 over NCP region. The NCP region was chosen because it is the key target region of air pollution control in China and where
332 unexpected COVID-19 haze occurred. A major caveat in previous studies that explored the impacts of COVID-19
333 lockdowns on air quality is the uncertainty in the emission changes during COVID-19 restrictions. The inversion results
334 enable us give a more reliable assessment of the environmental impacts of COVID-19 restrictions. Figure 8 shows the
335 observed changes in $PM_{2.5}$ and O_3 concentrations over the NCP region from the P1 to P2 period. The observations showed
336 consistent reductions in $PM_{2.5}$ concentrations over the NCP region (by $13.6 \mu\text{g}/\text{m}^3$). However, substantial increases in $PM_{2.5}$
337 concentrations were observed in the Beijing area (by $31.2 \mu\text{g}/\text{m}^3$). In contrast to the widespread reductions in $PM_{2.5}$
338 concentrations, the O_3 concentrations significantly increased over the whole NCP region (by $28.3 \mu\text{g}/\text{m}^3$) and the Beijing
339 area (by $16.8 \mu\text{g}/\text{m}^3$). The simulations based on our inversion results reproduced the observed changes in $PM_{2.5}$ and O_3
340 concentrations over the NCP region well, although the increases in O_3 concentrations were relatively overestimated in the
341 simulation (Fig. 7-8).

342 As detailed in the Sect 2.4, the simulated changes in air pollutant concentrations before and after lockdown were
343 decomposed into meteorological-induced (MI) changes and emission-induced (EI) changes through two different scenarios
344 to account for the nonlinearity of the atmospheric chemical system. The meteorological variation dominated the changes in
345 $PM_{2.5}$ concentrations over the NCP region (Fig. 9), which contributed 90% of the $PM_{2.5}$ reductions over most parts of the
346 NCP region. Moreover, this variation made significant contributions (57.9%) to the increases in $PM_{2.5}$ concentrations over
347 the Beijing area. This finding suggested that meteorological variations played an irreplaceable role in the occurrence of
348 COVID-19 haze around the Beijing area. Compared with the meteorological conditions before lockdown (Fig. 10), there
349 were increases in relative humidity over northern China, which facilitated the reactions for aerosol formation and growth.
350 Wind speed also decreased over the Beijing area accompanied by an anomalous south wind, which facilitated aerosol
351 accumulation and the transportation of air pollutants from the polluted industrial regions of the Hebei Province to Beijing.
352 The increases in boundary layer height from the P1 to P2 period were also much smaller in the Beijing area than in other
353 areas of the NCP. Thus, the Beijing area has exhibited distinct meteorological variations from other areas of the NCP region,
354 which correspond well to the different changes in $PM_{2.5}$ concentrations over the Beijing area.



355 The emission changes contributed slightly to the $PM_{2.5}$ reductions over the NCP region (8.6%). This is because, on the
356 one hand, the large reductions in NO_x emissions (by 44.4%) only reduced nitrate by approximately 10–30% due to the
357 nonlinear effects of chemical reactions (Fig. 11), and on the other hand, the emissions of primary $PM_{2.5}$ and its precursors
358 from other sectors changed little during the COVID-19 restrictions (Table 3). The emission changes contributed more to the
359 increased $PM_{2.5}$ concentrations over the Beijing area (42.1%). This is mainly associated with the increases in primary $PM_{2.5}$
360 emissions around the Beijing area, as seen in Fig. 6, possibly due to the increased emissions from firework during the Spring
361 Festival over the rural area of Beijing (Dai et al., 2020). Therefore, our results suggested that the unexpected COVID-19
362 haze was mainly driven by unfavorable meteorological conditions together with small changes or even increases in primary
363 $PM_{2.5}$ emissions. This finding is in line with previous results of Le et al. (2020) but different from those of Huang et al.
364 (2021), who suggested that enhanced secondary aerosol formation was the main driver of severe haze during the COVID-19
365 restrictions. To investigate it, we further analyzed the changes in the concentrations of secondary inorganic aerosols (SIAs).
366 First, we evaluated our model results against the observed SIA concentrations, which showed that the model results using
367 our inversion emissions well reproduced the observed concentrations of SIAs over the NCP region (Fig. 12) with mean bias
368 (MB) ranging from -5.14 to $5.45 \mu\text{g}/\text{m}^3$ and correlation coefficient (R) ranging from 0.59 to 0.80. The observed increases in
369 SIA concentrations over the Beijing area, especially for sulfate concentrations, were also captured in our simulations (Fig.
370 11), although underestimation occurred due to the uncertainty in simulating SIA concentrations. Through sensitivity
371 experiments, we found that the increases in SIA concentrations were still driven by meteorological variations (Fig. 13). In
372 fact, the emission reductions only led to a 10% decrease in SIA concentrations over the NCP region. This finding suggests
373 that the enhanced secondary aerosol formation was likely mainly driven by the unfavorable meteorological conditions
374 associated with higher temperature and relative humidity instead of the emission reductions during the lockdown period.
375 This is in line with the observation evidences from Ma, T et al (2022) who emphasized that the increased temperature and
376 relative humidity promoted the formation of secondary pollutants during the COVID-19 restrictions.

377 In terms of O_3 concentrations, the emission changes subsequently became the dominant contributor to the O_3 increases
378 by more than 100% in the Beijing area and by 96.0% over the NCP region. This result is mainly because the lockdown
379 period occurred in midwinter when photochemical O_3 formation was minimal; thus, the large increase in O_3 is expected
380 solely from the effect of the reduced titration reaction associated with the large reductions in NO_x emissions. Although the
381 higher temperature and slower wind speed during the lockdown period were favorable for the increases in O_3 concentrations,
382 their contributions were much smaller than those of emission changes (Fig. 9). These results suggested that control measures,
383 such as COVID-19 restrictions, were inefficient for air pollution mitigation in China considering the high economic cost of
384 the COVID-19 restrictions.



385 4 Conclusions

386 The COVID-19 pandemic is an unprecedented event that significantly influenced the social activity and associated
387 emissions of air pollutants. Our results provide a quantitative assessment of the influences of COVID-19 restrictions on
388 multi-air pollutant emissions in China. Otherwise, understanding of the relationship between air quality and human activities
389 may be biased. The inversion results provide important evidences that the COVID-19 lockdown policy was largely a traffic
390 control measure with substantially reducing impacts on NO_x emissions but much smaller influences on the emissions of other
391 species and other sectors. Traffic control has widely been considered to be the normal protocol in implementing regulations
392 in many cities of China, but its effectiveness on air pollution control is still disputed (Han and Naeher, 2006; Zhang et al.,
393 2007; Chen et al., 2021; Cai and Xie, 2011; Chowdhury et al., 2017; Li et al., 2017c). Thus, the COVID-19 restrictions
394 provided us with a real nationwide traffic control scenario to investigate the effectiveness of traffic control on the mitigation
395 of air pollution in China. The results suggested that traffic control as a separate pollution control measure has limited effects
396 on the coordinated control of high concentrations of O_3 and $\text{PM}_{2.5}$ under the current air pollution conditions in China. In this
397 case, the $\text{PM}_{2.5}$ concentrations were slightly reduced, while leading to substantial increases in O_3 concentrations. Severe haze
398 was also not avoided during the COVID-19 restrictions due to unbalanced emission changes from other sectors and
399 unfavorable meteorological conditions. China is now facing major challenges in both controlling $\text{PM}_{2.5}$ and controlling
400 emerging O_3 pollution. The tragic COVID-19 pandemic has revealed the limitation of the road traffic control measure in the
401 coordinated control of $\text{PM}_{2.5}$ and O_3 . More comprehensive regulations for multiple precursors from different sectors are
402 required in the future to address O_3 and $\text{PM}_{2.5}$ pollution in China.

403
404
405
406
407
408
409
410
411
412
413
414
415



416 **Tables**

417 **Table 1. Corresponding relationship between the chemical observations and adjusted emissions**

| Species | Descriptions | Observations that used for inversions of this species |
|-----------------|--------------------------------|---|
| BC | black carbon | PM _{2.5} |
| OC | organic carbon | PM _{2.5} |
| PMF | fine mode unspciated aerosol | PM _{2.5} |
| PMC | coarse mode unspciated aerosol | PM ₁₀ – PM _{2.5} |
| NO _x | nitrogen oxide | NO ₂ |
| SO ₂ | sulfur dioxide | SO ₂ |
| CO | carbon monoxide | CO |

418

419

420 **Table 2. Inversion estimated emissions of different air pollutants in China and their changes between different periods during**
421 **COVID-19.**

| | NO _x | SO ₂ | CO | PM _{2.5} | PM ₁₀ |
|-------------|-----------------|-----------------|--------|-------------------|------------------|
| P1 (Gg/day) | 72.9 | 23.8 | 1160.2 | 44.5 | 75.5 |
| P2 (Gg/day) | 41.9 | 21.5 | 1037.4 | 40.9 | 66.4 |
| P3 (Gg/day) | 44.8 | 23.2 | 1078.2 | 45.9 | 108.4 |
| (P2-P1)/P1 | -42.5% | -9.7% | -10.6% | -7.9% | -12.1% |
| (P3-P2)/P1 | 3.9% | 7.2% | 3.6% | 11.2% | 55.7% |
| (P3-P1)/P1 | -38.6% | -2.5% | -7.0% | 3.3% | 43.6% |

422

423

424

425

426

427

428

429

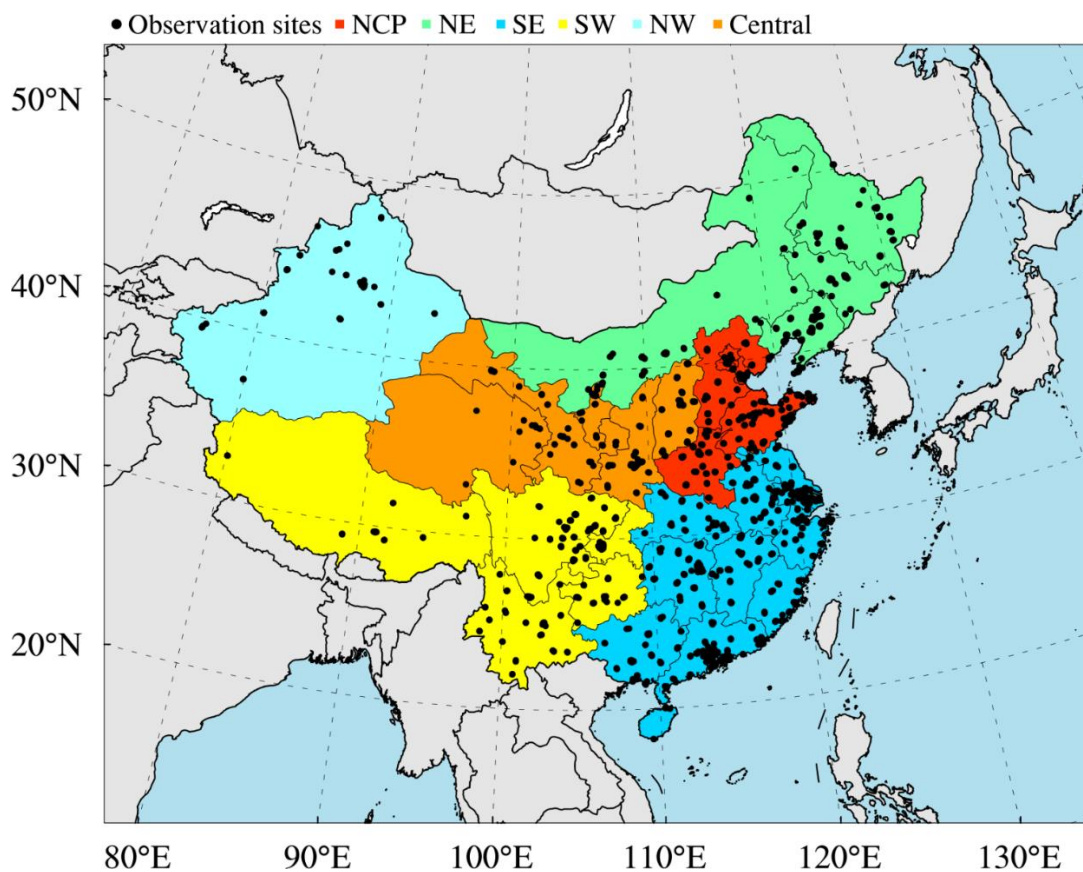


430 **Table 3. Inversion estimated emission changes of different air pollutants over different regions in China between different periods**
 431 **during COVID-19 restrictions**

| | NO _x | PM _{2.5} | PM ₁₀ | SO ₂ | CO |
|------------|-----------------|-------------------|------------------|-----------------|--------|
| NCP | | | | | |
| (P2-P1)/P1 | -44.4% | 5.5% | 2.8% | -1.6% | -4.3% |
| (P3-P2)/P1 | -0.8% | -9.9% | 31.8% | -5.9% | -10.0% |
| (P3-P1)/P1 | -45.2% | -4.3% | 34.7% | -7.5% | -14.3% |
| NE | | | | | |
| (P2-P1)/P1 | -41.8% | -8.8% | -3.5% | -3.2% | -10.9% |
| (P3-P2)/P1 | -6.0% | -19.2% | 23.7% | -2.9% | -6.6% |
| (P3-P1)/P1 | -47.8% | -28.0% | 20.2% | -6.1% | -17.5% |
| SE | | | | | |
| (P2-P1)/P1 | -41.4% | -9.5% | -24.4% | -19.4% | -3.5% |
| (P3-P2)/P1 | 10.2% | 12.3% | 28.6% | 19.8% | 13.1% |
| (P3-P1)/P1 | -31.2% | 2.8% | 4.2% | 0.3% | 9.7% |
| SW | | | | | |
| (P2-P1)/P1 | -43.5% | -12.6% | -25.9% | -17.5% | -23.8% |
| (P3-P2)/P1 | 6.0% | 47.7% | 33.1% | 7.5% | 7.4% |
| (P3-P1)/P1 | -37.5% | 35.1% | 7.2% | -10.0% | -16.4% |
| NW | | | | | |
| (P2-P1)/P1 | -38.5% | -4.0% | -8.3% | 14.2% | -2.6% |
| (P3-P2)/P1 | -21.1% | 4.9% | 145.3% | -4.1% | -7.2% |
| (P3-P1)/P1 | -59.6% | 0.9% | 136.9% | 10.1% | -9.8% |
| Central | | | | | |
| (P2-P1)/P1 | -43.8% | -23.7% | -15.7% | -10.6% | -17.4% |
| (P3-P2)/P1 | 16.4% | 24.4% | 135.9% | 18.5% | 8.4% |
| (P3-P1)/P1 | -27.4% | 0.7% | 120.3% | 7.9% | -9.0% |

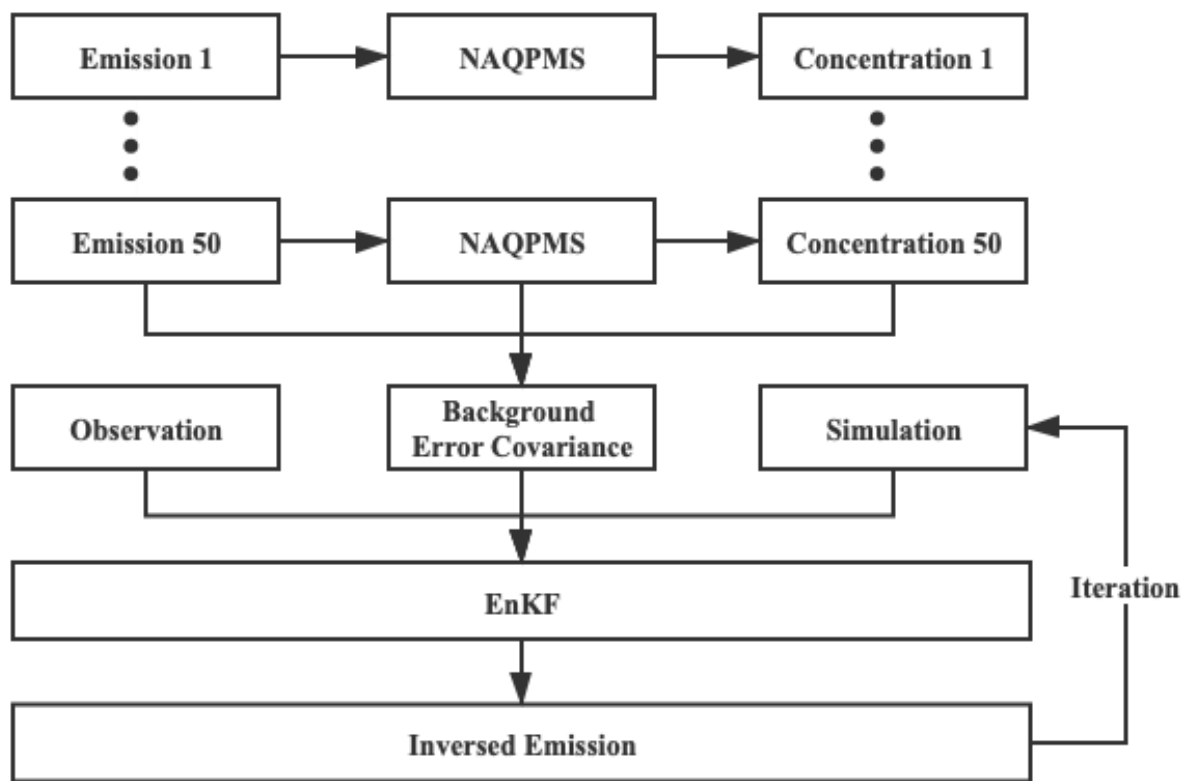


432 **Figures**



433

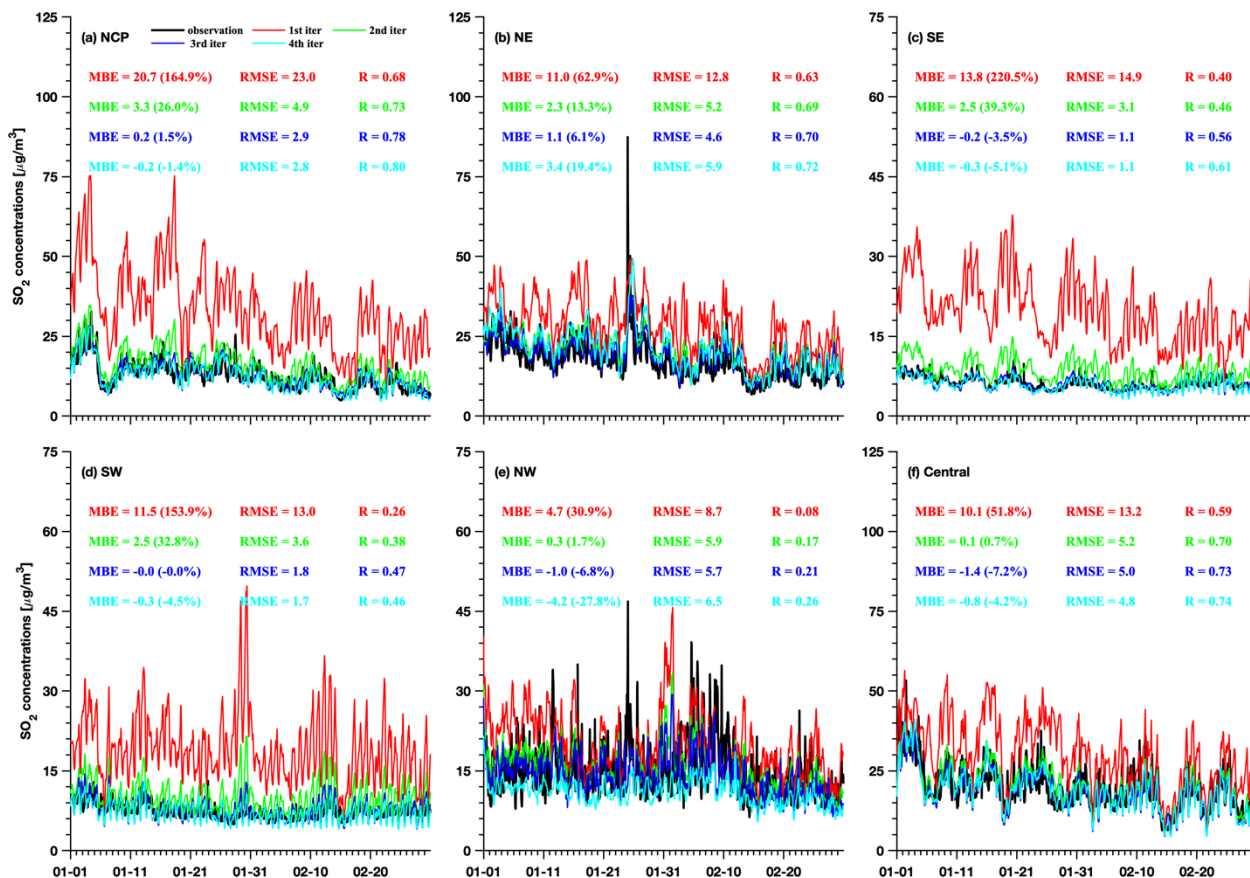
434 **Figure 1: Modeling domain of the ensemble simulation overlay the distributions of observation sites from CNEMC. Different**
435 **colours denote the different regions in mainland of China, namely North China Plain (NCP), Northeast China (NE), Southwest**
436 **China (SW), Southeast China (SE), Northwest China (NW) and Central.**



437

438 **Figure 2: Illustration of the iteration inversion scheme used in this study.**

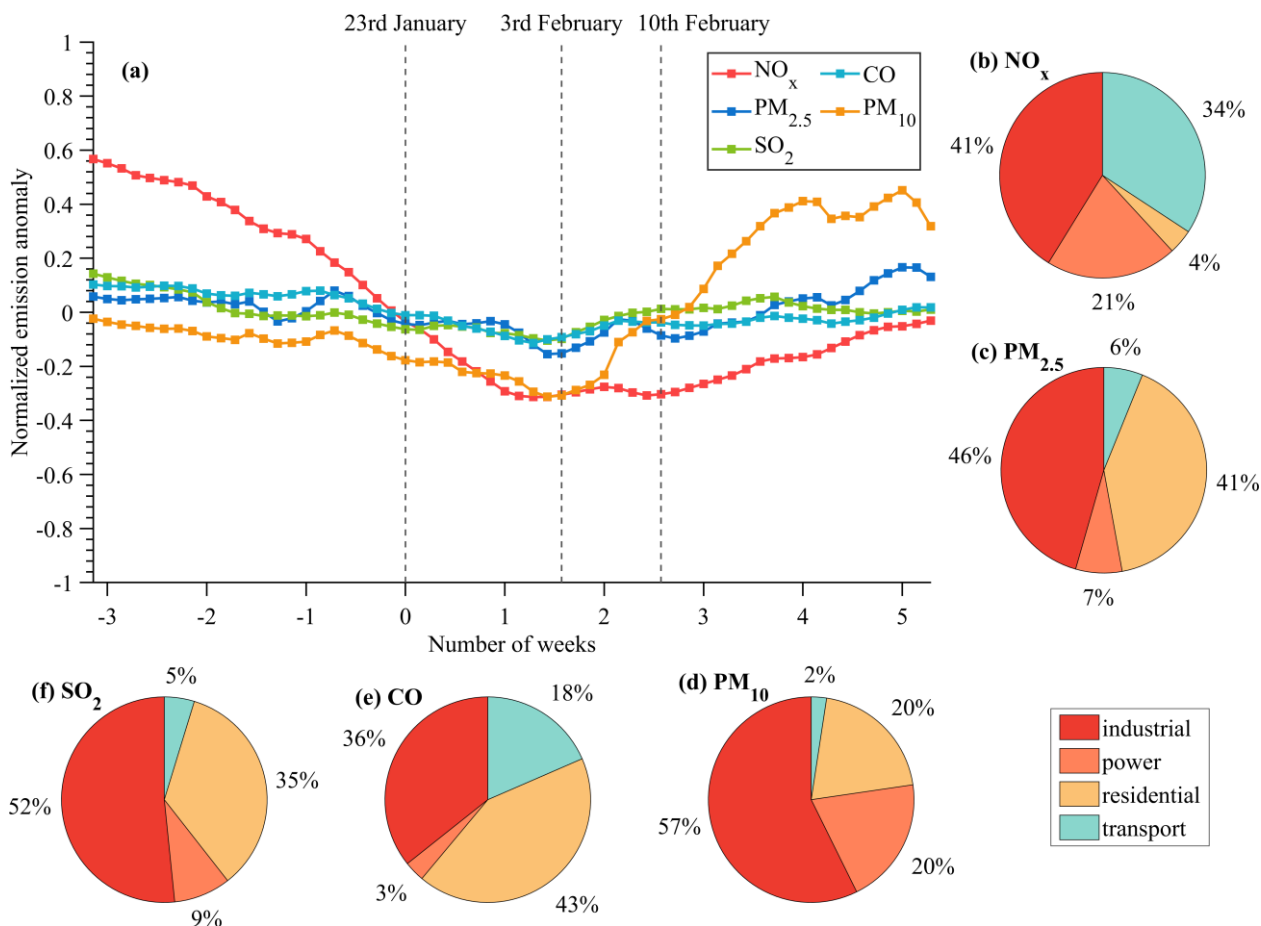
439



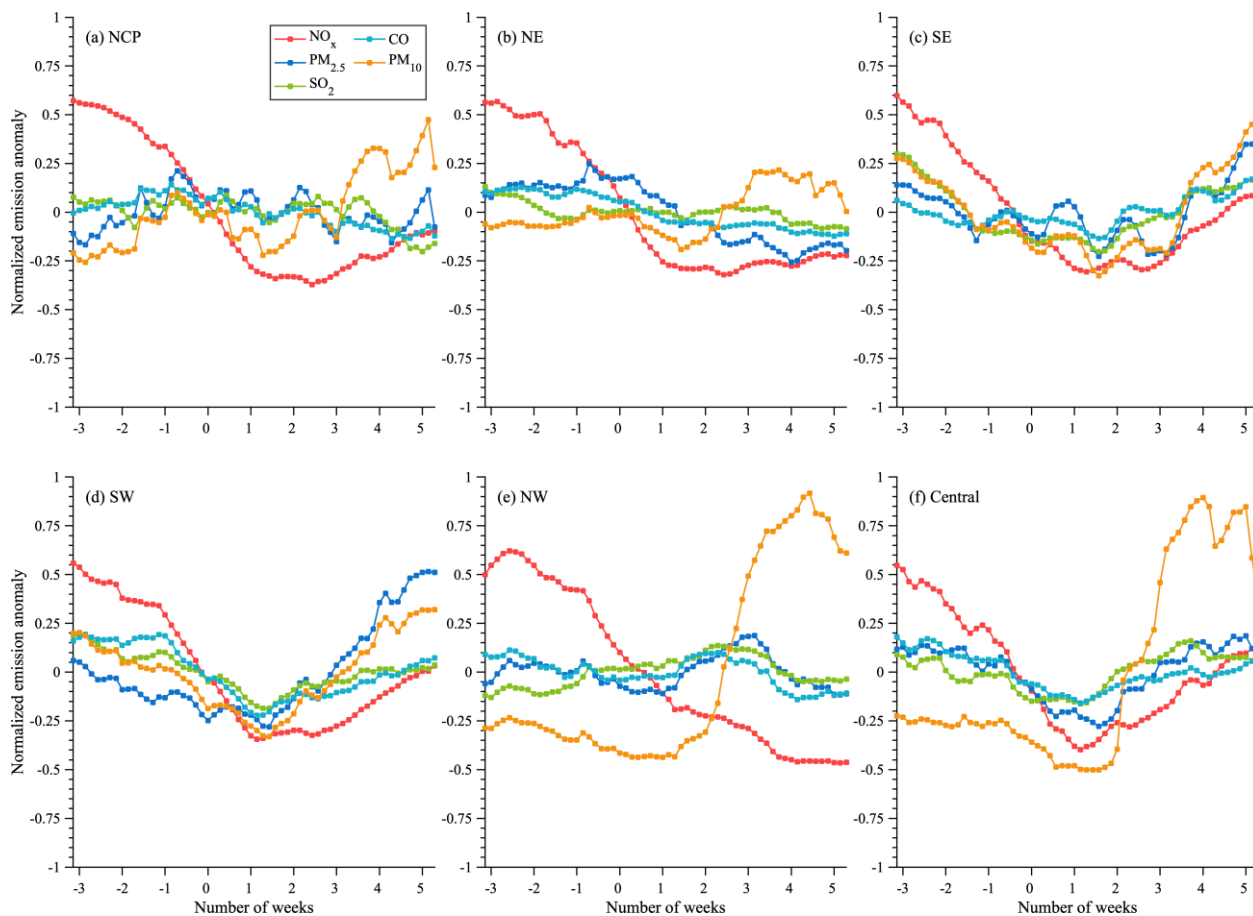
440

441 **Figure 3: Comparisons of the observed and simulated mean SO₂ concentrations using emissions of different iteration time at**
 442 **validation sites over (a) NCP region, (b) NE region, (c) SE region, (d) SW region, (e) NW region and (f) Central region.**

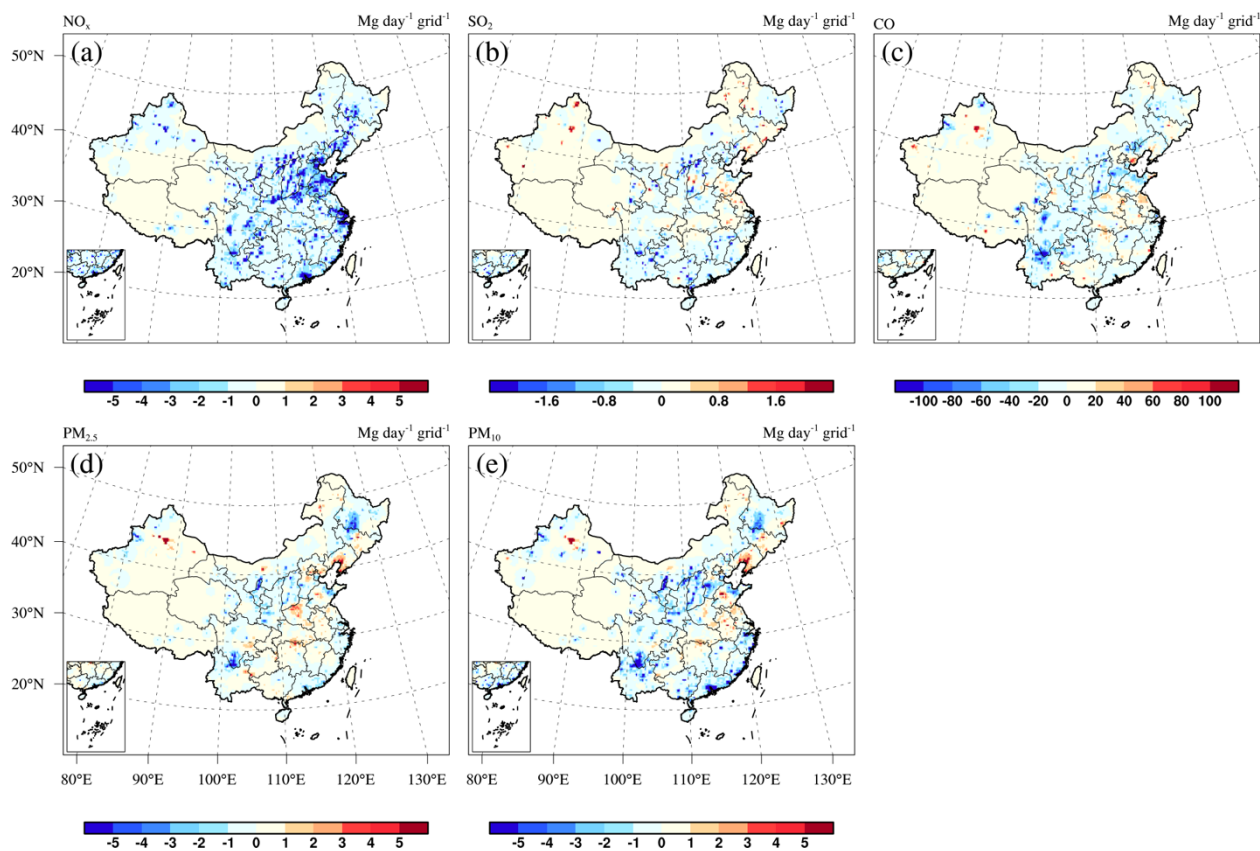
443



444
 445 **Figure 4: (a) Time series of normalized emission anomalies estimated by inversion results for different species in China from 1st**
 446 **January to 29th February 2020, and (b-f) Relative contributions of different sectors to the total anthropogenic emissions of NO_x,**
 447 **PM_{2.5}, PM₁₀, CO and SO₂ obtained from Zheng et al. (2018). The normalized emission anomaly is calculated by the emission**
 448 **anomaly divided by the average emissions during the whole period.**

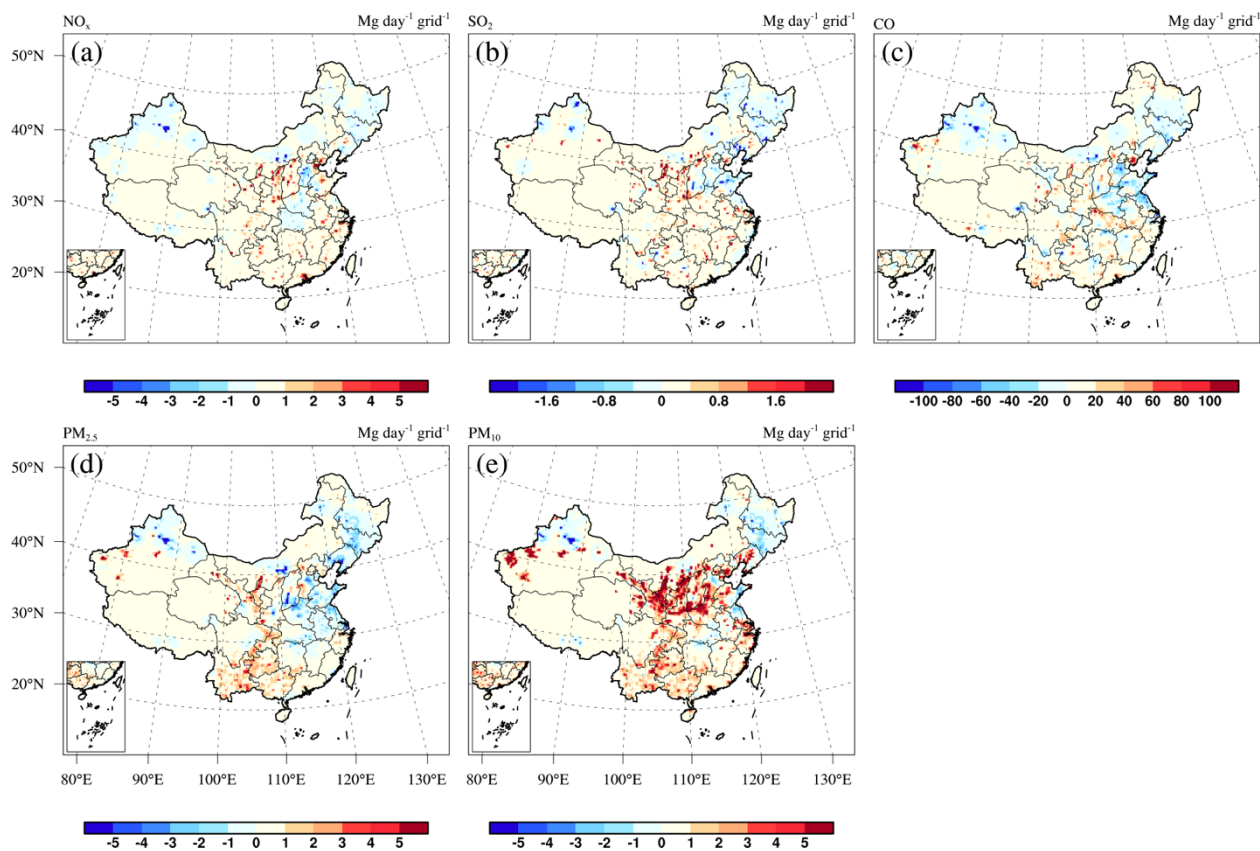


449
450 **Figure 5: Time series of normalized emission anomalies estimated by inversion results for different species over (a) NCP region, (b)**
451 **NE region, (c) SE region, (d) SW region, (e) NW region and (f) Central region from 1st January to 29th February 2020.**



452

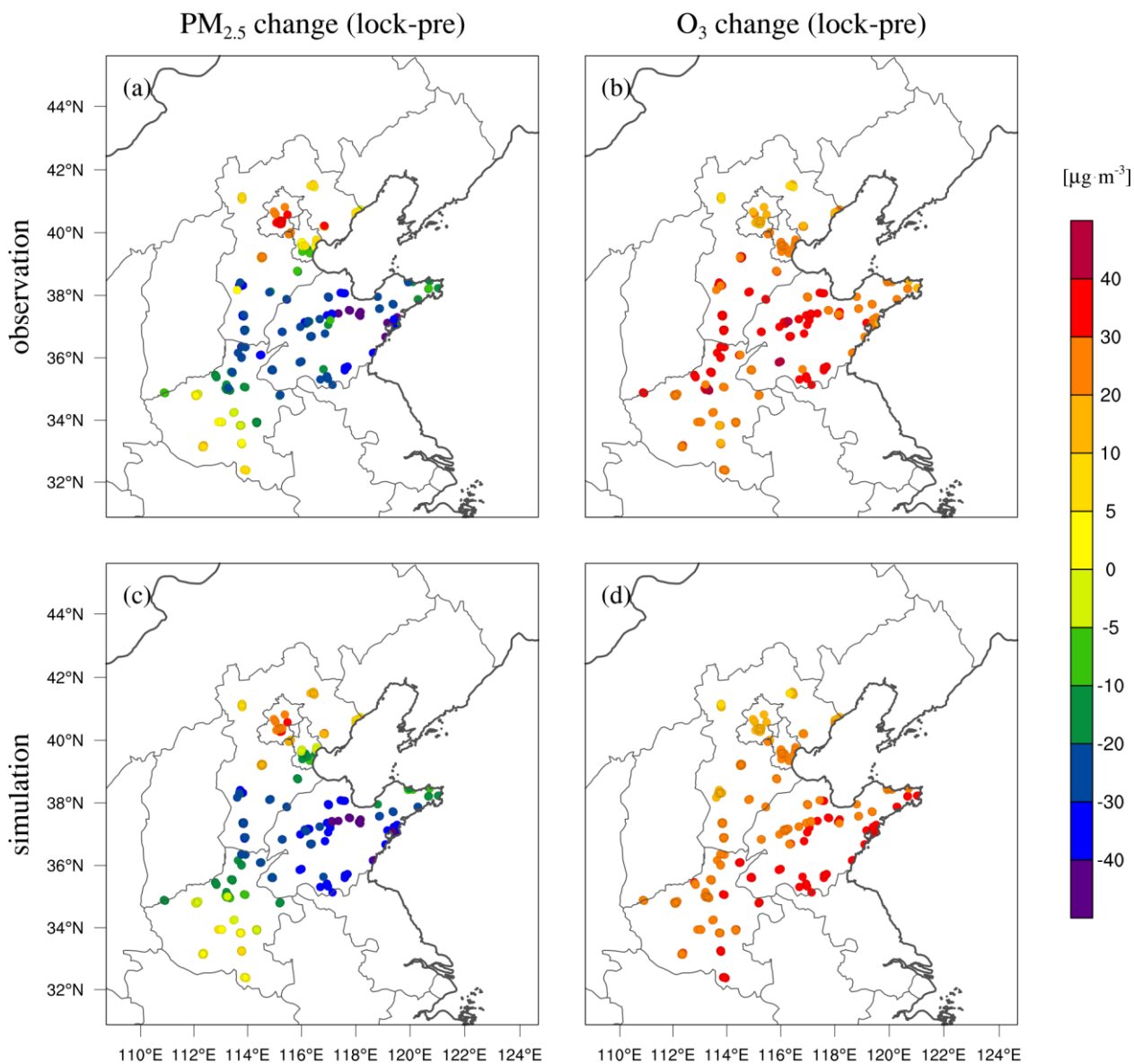
453 **Figure 6:** The inversion estimated emission changes of (a) NO_x , (b) SO_2 , (c) CO , (d) $\text{PM}_{2.5}$ and (e) PM_{10} in China from P1 to P2
454 period.



455

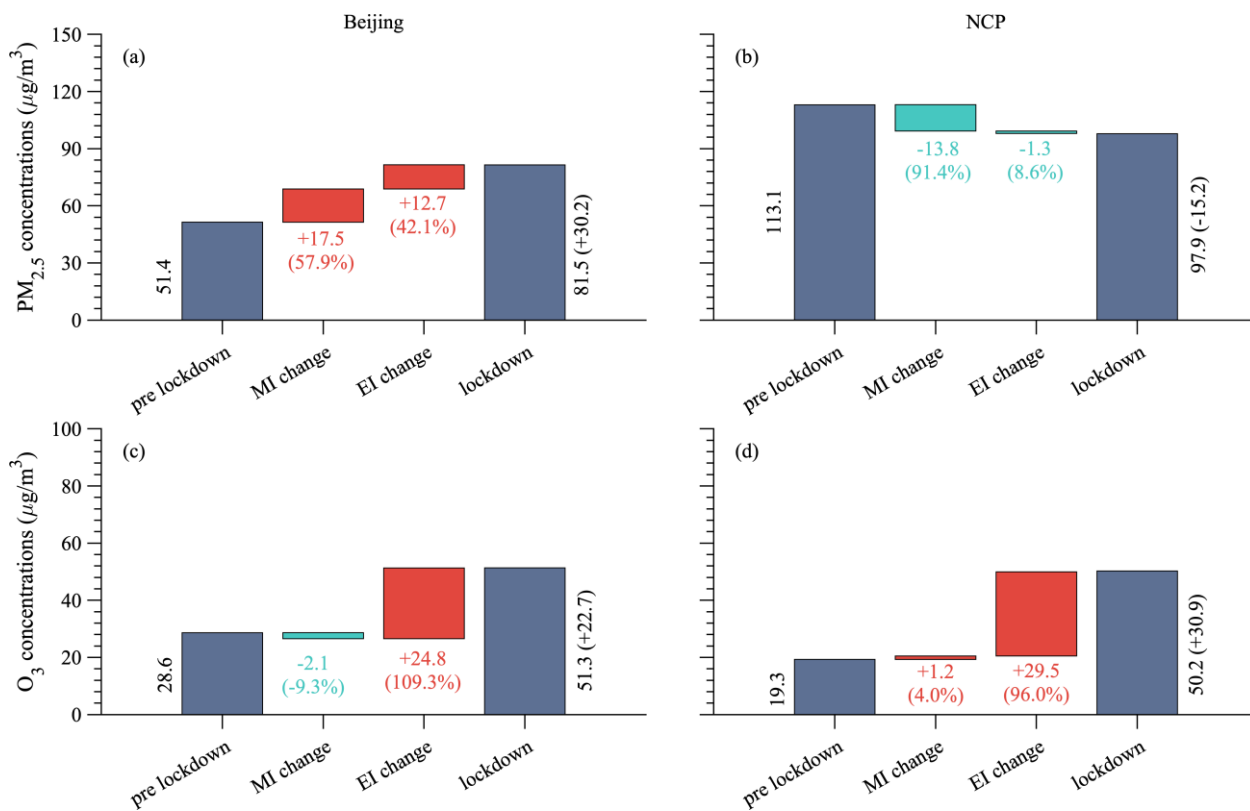
456 **Figure 7: The inversion estimated emission changes of (a) NO_x , (b) SO_2 , (c) CO, (d) $\text{PM}_{2.5}$ and (e) PM_{10} in China from P2 to P3**
457 **period.**

458



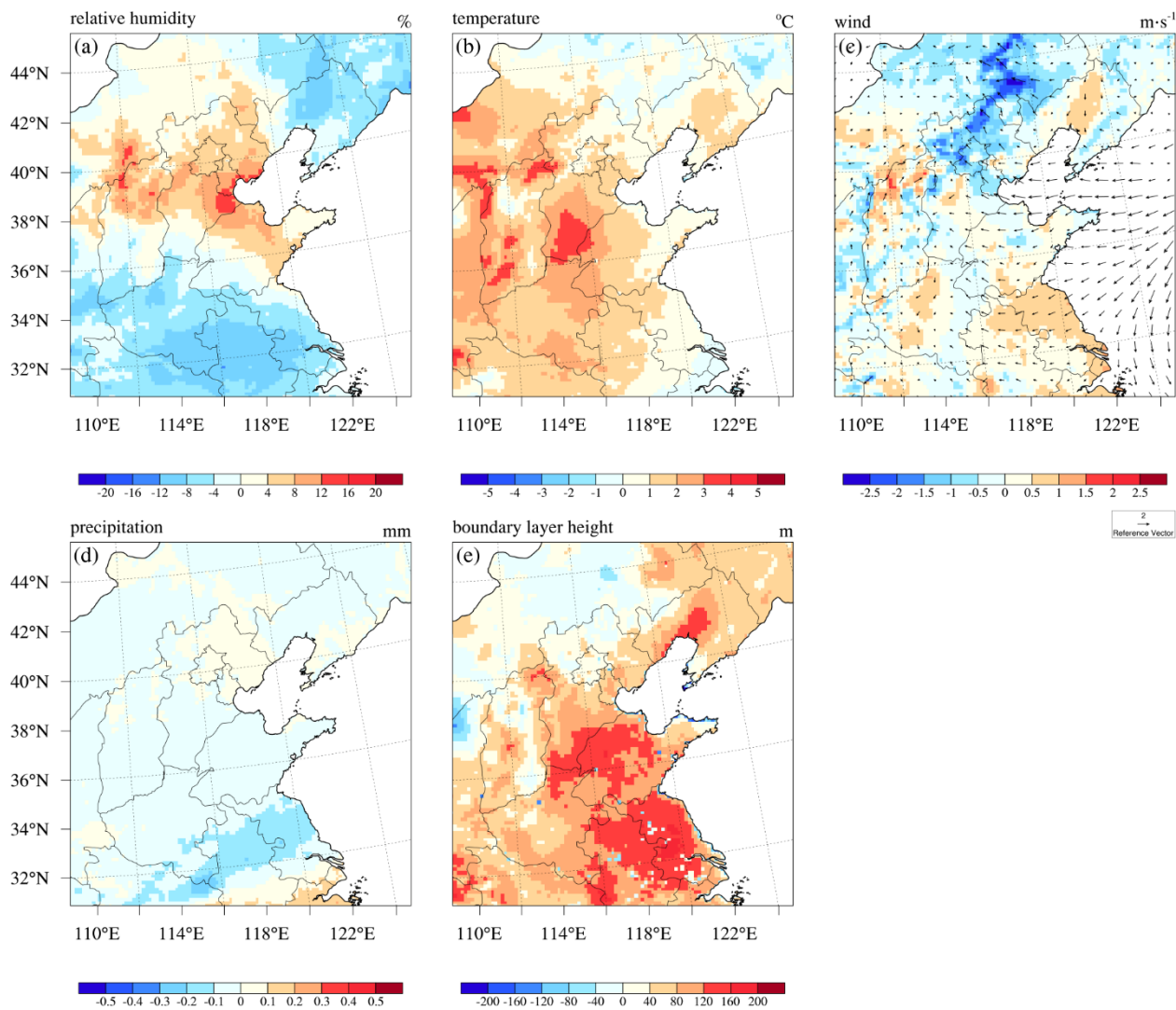
459

460 **Figure 8:** Changes in the observed and simulated concentrations of (a, c) $\text{PM}_{2.5}$ and (b, d) O_3 over the NCP region from the pre
461 lockdown period (P1) to the lockdown period (P2).



462

463 **Figure 9: Contributions of the meteorological variations and emission changes to the changes in (a, b) $\text{PM}_{2.5}$ and (c, d) O_3**
 464 **concentrations over Beijing and the NCP region from the pre lockdown period (P1) to the lockdown period (P2).**



465

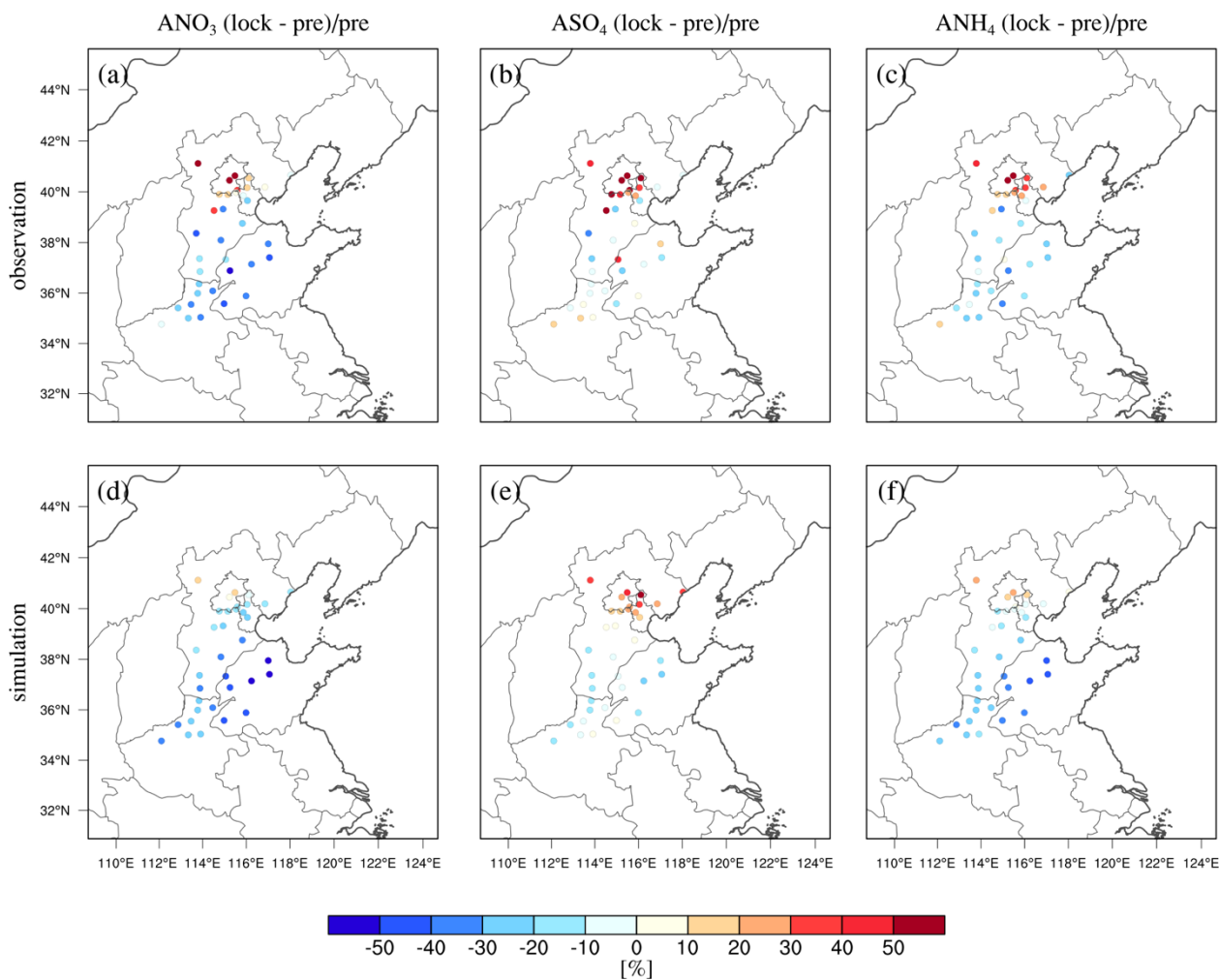
466 **Figure 10: Changes in the (a) relative humidity, (b) temperature, (c) wind speed, (d) precipitation and (e) boundary layer height**
467 **over the NCP region from P1 to P2 period obtained from WRF simulations.**

468

469

470

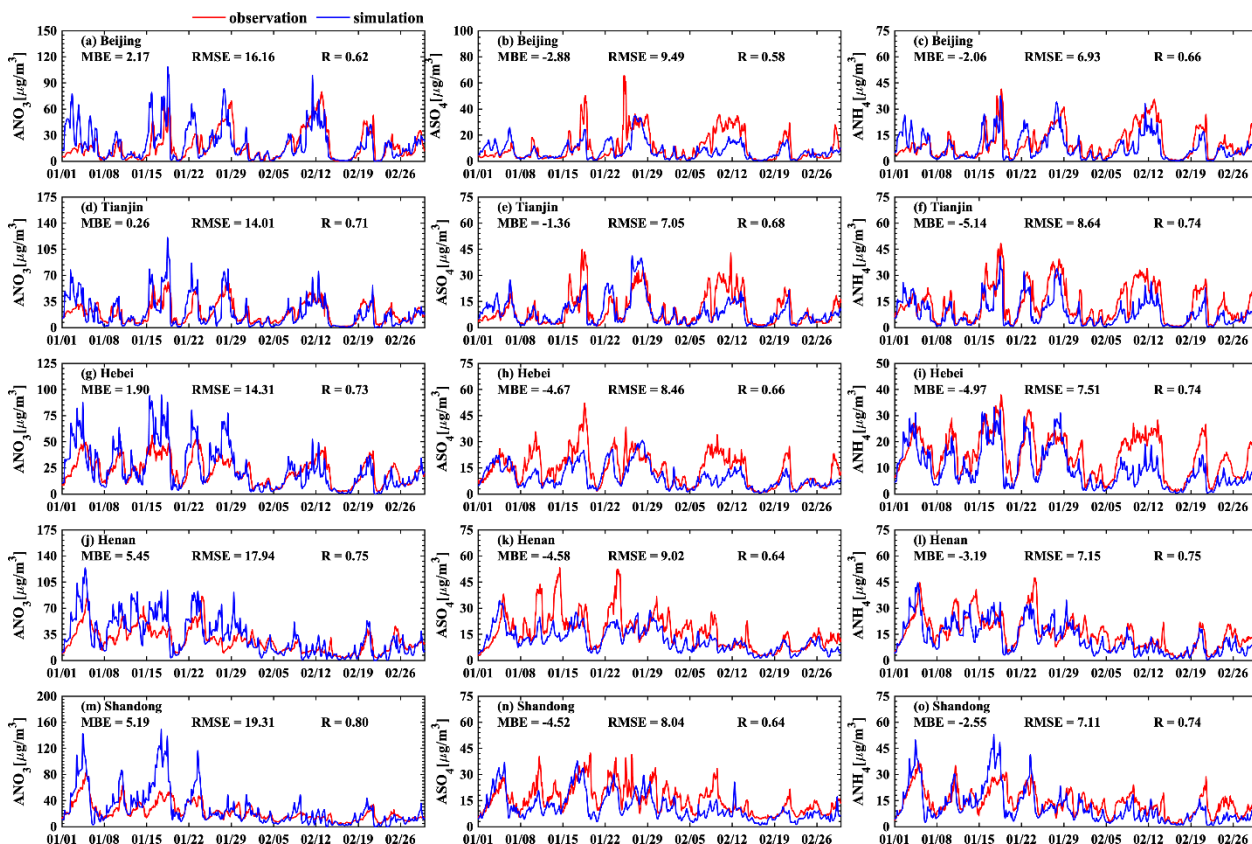
471



472

473 **Figure 11: Relative changes in the simulated and observed concentrations of (a) ANO_3 , (b) ASO_4 , (c) ANH_4 over NCP region from**
474 **P1 to P2 period.**

475

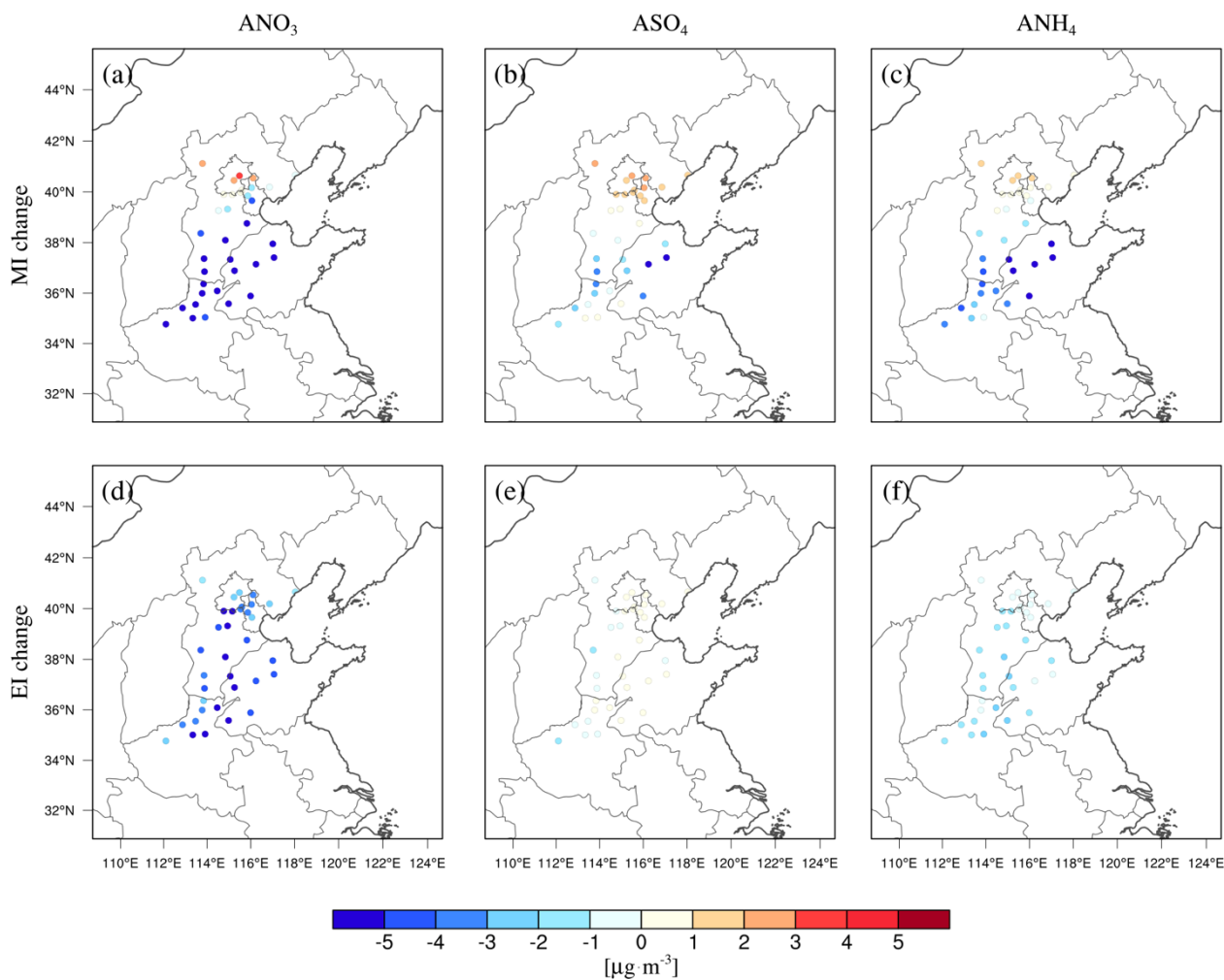


476

477 **Figure 12:** Time series of observed and simulated concentrations of ANO₃, ASO₄ and ANH₄ in (a-c) Beijing, (b-f) Tianjin, (g-i)
478 Hebei, (j-l) Henan and (m-o) Shangdong province from 1st January to 29th February 2020.

479

480



481

482 **Figure 13: Meteorology-induced (MI) changes in the concentrations of (a) ANO_3 , (b) ASO_4 and (c) ANH_4 , as well as Emission-**
483 **induced (EI) changes in the concentrations of (d) ANO_3 , (e) ASO_4 and (f) ANH_4 .**

484

485 **Data availability**

486 The hourly surface observations can be obtained from China National Environmental Monitoring Centre
487 (<http://www.cnemc.cn/en>); The inversion estimated emissions of multi-air pollutants in China during COVID-19 lockdown
488 period and the NAQPMS simulation results are available from the corresponding authors on request.



489 **Author contributions**

490 X.T., J.Z., and Z.W. conceived and designed the project; H.W., L.K., X.T., and L.W. established the data assimilation
491 system; M.L. Q.W. S.H. W.S. contributed to interpreting the data. L.K. conducted the inversion estimate, drew figures, and
492 wrote the paper with comments provided by J.L., X.P., M.G., P.F., Y.S., H.A. and G.R.C.

493 **Competing interests**

494 The authors declare no competing financial interest.

495 **Acknowledgements**

496 We acknowledge the use of surface air quality observation data from CNEMC. This study has been supported by the
497 National Natural Science Foundation of China (grant nos. 41875164, 91644216, 92044303), the CAS Strategic Priority
498 Research Program (grant no. XDA19040201), the CAS Information Technology Program (grant no. XXH13506-302), and
499 the National Key Scientific and Technological Infrastructure project “Earth System Science Numerical Simulator Facility”
500 (EarthLab).

501 **References**

- 502 Brasseur, G. P., Hauglustaine, D. A., Walters, S., Rasch, P. J., Muller, J. F., Granier, C., and Tie, X. X.: MOZART, a global chemical
503 transport model for ozone and related chemical tracers 1. Model description, *J. Geophys. Res.-Atmos.*, 103, 28265-28289,
504 <https://doi.org/10.1029/98jd02397>, 1998.
- 505 Cai, H. and Xie, S.: Traffic-related air pollution modeling during the 2008 Beijing Olympic Games: The effects of an odd-even day traffic
506 restriction scheme, *Sci. Total Environ.*, 409, 1935-1948, <https://doi.org/10.1016/j.scitotenv.2011.01.025>, 2011.
- 507 Chen, Z., Hao, X., Zhang, X., and Chen, F.: Have traffic restrictions improved air quality? A shock from COVID-19, *J. Clean Prod.*, 279,
508 123622, <https://doi.org/10.1016/j.jclepro.2020.123622>, 2021.
- 509 Cheng, C., Barceló, J., Hartnett, A. S., Kubinec, R., and Messerschmidt, L.: COVID-19 Government Response Event Dataset (CoronaNet
510 v.1.0), *Nat. Hum. Behav.*, 4, 756-768, <https://doi.org/10.1038/s41562-020-0909-7>, 2020.
- 511 Chowdhury, S., Dey, S., Tripathi, S. N., Beig, G., Mishra, A. K., and Sharma, S.: “Traffic intervention” policy fails to mitigate air pollution
512 in megacity Delhi, *Environ. Sci. Policy*, 74, 8-13, <https://doi.org/10.1016/j.envsci.2017.04.018>, 2017.
- 513 Chu, B., Zhang, S., Liu, J., Ma, Q., and He, H.: Significant concurrent decrease in PM_{2.5} and NO₂ concentrations in China during COVID-
514 19 epidemic, *J. Environ. Sci.*, 99, 346-353, <https://doi.org/10.1016/j.jes.2020.06.031>, 2021.
- 515 Chu, K. K., Peng, Z., Liu, Z. Q., Lei, L. L., Kou, X. X., Zhang, Y., Bo, X., and Tian, J.: Evaluating the Impact of Emissions Regulations on
516 the Emissions Reduction During the 2015 China Victory Day Parade With an Ensemble Square Root Filter, *J. Geophys. Res.-Atmos.*,
517 123, 4122-4134, <https://doi.org/10.1002/2017jd027631>, 2018.



- 518 Dai, Q., Liu, B., Bi, X., Wu, J., Liang, D., Zhang, Y., Feng, Y., and Hopke, P. K.: Dispersion Normalized PMF Provides Insights into the
519 Significant Changes in Source Contributions to PM_{2.5} after the COVID-19 Outbreak, *Environ. Sci. Technol.*, 54, 9917-9927,
520 <https://doi.org/10.1021/acs.est.0c02776>, 2020.
- 521 Diamond, M. S. and Wood, R.: Limited Regional Aerosol and Cloud Microphysical Changes Despite Unprecedented Decline in Nitrogen
522 Oxide Pollution During the February 2020 COVID-19 Shutdown in China, *Geophys. Res. Lett.*, 47, e2020GL088913,
523 <https://doi.org/10.1029/2020gl088913>, 2020.
- 524 Evensen, G.: Sequential data assimilation with a nonlinear quasi-geostrophic model using Monte Carlo methods to forecast error statistics,
525 *J. Geophys. Res.-Oceans*, 99, 10143-10162, <https://doi.org/10.1029/94JC00572>, 1994.
- 526 Fan, C., Li, Y., Guang, J., Li, Z. Q., Elnashar, A., Allam, M., and de Leeuw, G.: The Impact of the Control Measures during the COVID-19
527 Outbreak on Air Pollution in China, *Remote Sens.*, 12, 23, <https://doi.org/10.3390/rs12101613>, 2020.
- 528 Feng, S., Jiang, F., Wang, H., Wang, H., Ju, W., Shen, Y., Zheng, Y., Wu, Z., and Ding, A.: NO_x Emission Changes Over China During the
529 COVID-19 Epidemic Inferred From Surface NO₂ Observations, *Geophys. Res. Lett.*, 47, e2020GL090080, [10.1029/2020gl090080](https://doi.org/10.1029/2020gl090080), 2020.
- 530 Forster, P. M., Forster, H. I., Evans, M. J., Gidden, M. J., Jones, C. D., Keller, C. A., Lamboll, R. D., Le Quere, C., Rogelj, J., Rosen, D.,
531 Schuessler, C. F., Richardson, T. B., Smith, C. J., and Turnock, S. T.: Current and future global climate impacts resulting from COVID-
532 19, *Nat. Clim. Chang.*, 10, 913+, <https://doi.org/10.1038/s41558-020-0883-0>, 2020.
- 533 Granier, C., Lamarque, J., Mieville, A., Muller, J., Olivier, J., Orlando, J., Peters, J., Petron, G., Tyndall, G., and Wallens, S.: POET, a
534 database of surface emissions of ozone precursors, 2005.
- 535 Hammer, M. S., van Donkelaar, A., Martin, R. V., McDuffie, E. E., Lyapustin, A., Sayer, A. M., Hsu, N. C., Levy, R. C., Garay, M. J.,
536 Kalashnikova, O. V., and Kahn, R. A.: Effects of COVID-19 lockdowns on fine particulate matter concentrations, *Sci. Adv.*, 7,
537 <https://doi.org/10.1126/sciadv.abg7670>, 2021.
- 538 Han, X. L. and Naeher, L. P.: A review of traffic-related air pollution exposure assessment studies in the developing world, *Environ. Int.*, 32,
539 106-120, <https://doi.org/10.1016/j.envint.2005.05.020>, 2006.
- 540 Hauglustaine, D. A., Brasseur, G. P., Walters, S., Rasch, P. J., Muller, J. F., Emmons, L. K., and Carroll, C. A.: MOZART, a global
541 chemical transport model for ozone and related chemical tracers 2. Model results and evaluation, *J. Geophys. Res.-Atmos.*, 103, 28291-
542 28335, <https://doi.org/10.1029/98jd02398>, 1998.
- 543 He, G. J., Pan, Y. H., and Tanaka, T.: The short-term impacts of COVID-19 lockdown on urban air pollution in China, *Nat. Sustain.*, 3, 9,
544 <https://doi.org/10.1038/s41893-020-0581-y>, 2020.
- 545 Hu, Y., Zang, Z., Ma, X., Li, Y., Liang, Y., You, W., Pan, X., and Li, Z.: Four-dimensional variational assimilation for SO₂ emission and
546 its application around the COVID-19 lockdown in the spring 2020 over China, *Atmos. Chem. Phys.*, 22, 13183-13200,
547 <https://doi.org/10.5194/acp-22-13183-2022>, 2022.
- 548 Huang, X., Ding, A., Gao, J., Zheng, B., Zhou, D., Qi, X., Tang, R., Wang, J., Ren, C., Nie, W., Chi, X., Xu, Z., Chen, L., Li, Y., Che, F.,
549 Pang, N., Wang, H., Tong, D., Qin, W., Cheng, W., Liu, W., Fu, Q., Liu, B., Chai, F., Davis, S. J., Zhang, Q., and He, K.: Enhanced
550 secondary pollution offset reduction of primary emissions during COVID-19 lockdown in China, *Natl. Sci. Rev.*, 8,
551 <https://doi.org/10.1093/nsr/nwaa137>, 2021.
- 552 Janssens-Maenhout, G., Crippa, M., Guizzardi, D., Dentener, F., Muntean, M., Pouliot, G., Keating, T., Zhang, Q., Kurokawa, J.,
553 Wankmuller, R., van der Gon, H. D., Kuenen, J. J. P., Klimont, Z., Frost, G., Darras, S., Koffi, B., and Li, M.: HTAP_v2.2: a mosaic of
554 regional and global emission grid maps for 2008 and 2010 to study hemispheric transport of air pollution, *Atmos. Chem. Phys.*, 15,
555 11411-11432, <https://doi.org/10.5194/acp-15-11411-2015>, 2015.



- 556 Kong, L., Tang, X., Zhu, J., Wang, Z., Pan, Y., Wu, H., Wu, L., Wu, Q., He, Y., Tian, S., Xie, Y., Liu, Z., Sui, W., Han, L., and Carmichael,
557 G.: Improved Inversion of Monthly Ammonia Emissions in China Based on the Chinese Ammonia Monitoring Network and Ensemble
558 Kalman Filter, *Environ. Sci. Technol.*, 53, 12529-12538, <https://doi.org/10.1021/acs.est.9b02701>, 2019.
- 559 Kong, L., Tang, X., Zhu, J., Wang, Z., Li, J., Wu, H., Wu, Q., Chen, H., Zhu, L., Wang, W., Liu, B., Wang, Q., Chen, D., Pan, Y., Song, T.,
560 Li, F., Zheng, H., Jia, G., Lu, M., Wu, L., and Carmichael, G. R.: A 6-year-long (2013–2018) high-resolution air quality reanalysis
561 dataset in China based on the assimilation of surface observations from CNEMC, *Earth Syst. Sci. Data*, 13, 529-570,
562 <https://doi.org/10.5194/essd-13-529-2021>, 2021.
- 563 Le, T. H., Wang, Y., Liu, L., Yang, J. N., Yung, Y. L., Li, G. H., and Seinfeld, J. H.: Unexpected air pollution with marked emission
564 reductions during the COVID-19 outbreak in China, *Science*, 369, 702–+, <https://doi.org/10.1126/science.abb7431>, 2020.
- 565 Levelt, P. F., Stein Zweers, D. C., Aben, I., Bauwens, M., Borsdorff, T., De Smedt, I., Eskes, H. J., Lerot, C., Loyola, D. G., Romahn, F.,
566 Stavrou, T., Theys, N., Van Roozendaal, M., Veeffkind, J. P., and Verhoelst, T.: Air quality impacts of COVID-19 lockdown measures
567 detected from space using high spatial resolution observations of multiple trace gases from Sentinel-5P/TROPOMI, *Atmos. Chem. Phys.*,
568 22, <https://doi.org/10319-10351>, 10.5194/acp-22-10319-2022, 2022.
- 569 Li, F., Tang, X., Wang, Z., Zhu, L., Wang, X., Wu, H., Lu, M., Li, J., and Zhu, J.: Estimation of Representative Errors of Surface
570 Observations of Air Pollutant Concentrations Based on High-Density Observation Network over Beijing-Tianjin-Hebei Region, *Chinese
571 Journal of Atmospheric Sciences*, 43, 277-284, 2019.
- 572 Li, L., Li, Q., Huang, L., Wang, Q., Zhu, A., Xu, J., Liu, Z., Li, H., Shi, L., Li, R., Azari, M., Wang, Y., Zhang, X., Liu, Z., Zhu, Y., Zhang,
573 K., Xue, S., Ooi, M. C. G., Zhang, D., and Chan, A.: Air quality changes during the COVID-19 lockdown over the Yangtze River Delta
574 Region: An insight into the impact of human activity pattern changes on air pollution variation, *Sci. Total Environ.*, 732, 139282,
575 <https://doi.org/10.1016/j.scitotenv.2020.139282>, 2020.
- 576 Li, M., Wang, T., Xie, M., Li, S., Zhuang, B., Fu, Q., Zhao, M., Wu, H., Liu, J., Saikawa, E., and Liao, K.: Drivers for the poor air quality
577 conditions in North China Plain during the COVID-19 outbreak, *Atmos. Environ.*, 246, 118103,
578 <https://doi.org/10.1016/j.atmosenv.2020.118103>, 2021.
- 579 Li, M., Liu, H., Geng, G. N., Hong, C. P., Liu, F., Song, Y., Tong, D., Zheng, B., Cui, H. Y., Man, H. Y., Zhang, Q., and He, K. B.:
580 Anthropogenic emission inventories in China: a review, *Natl. Sci. Rev.*, 4, 834-866, <https://doi.org/10.1093/nsr/nwx150>, 2017a.
- 581 Li, M., Zhang, Q., Kurokawa, J. I., Woo, J. H., He, K., Lu, Z., Ohara, T., Song, Y., Streets, D. G., Carmichael, G. R., Cheng, Y., Hong, C.,
582 Huo, H., Jiang, X., Kang, S., Liu, F., Su, H., and Zheng, B.: MIX: a mosaic Asian anthropogenic emission inventory under the
583 international collaboration framework of the MICS-Asia and HTAP, *Atmos. Chem. Phys.*, 17, 935-963, <https://doi.org/10.5194/acp-17-935-2017>, 2017b.
- 585 Li, X., Zhang, Q., Zhang, Y., Zhang, L., Wang, Y. X., Zhang, Q. Q., Li, M., Zheng, Y. X., Geng, G. N., Wallington, T. J., Han, W. J., Shen,
586 W., and He, K. B.: Attribution of PM_{2.5} exposure in Beijing-Tianjin-Hebei region to emissions: implication to control strategies, *Sci.
587 Bull.*, 62, 957-964, <https://doi.org/10.1016/j.scib.2017.06.005>, 2017c.
- 588 Ma, C. Q., Wang, T. J., Mizzi, A. P., Anderson, J. L., Zhuang, B. L., Xie, M., and Wu, R. S.: Multiconstituent Data Assimilation With
589 WRF-Chem/DART: Potential for Adjusting Anthropogenic Emissions and Improving Air Quality Forecasts Over Eastern China, *J.
590 Geophys. Res.-Atmos.*, 124, 7393-7412, <https://doi.org/10.1029/2019jd030421>, 2019.
- 591 Miyazaki, K., Eskes, H. J., Sudo, K., Takigawa, M., van Weele, M., and Boersma, K. F.: Simultaneous assimilation of satellite NO₂, O₃,
592 CO, and HNO₃ data for the analysis of tropospheric chemical composition and emissions, *Atmos. Chem. Phys.*, 12, 9545-9579,
593 <https://doi.org/10.5194/acp-12-9545-2012>.



- 594 Okuda, T., Matsuura, S., Yamaguchi, D., Umemura, T., Hanada, E., Orihara, H., Tanaka, S., He, K., Ma, Y., Cheng, Y., and Liang, L.: The
595 impact of the pollution control measures for the 2008 Beijing Olympic Games on the chemical composition of aerosols, *Atmos. Environ.*,
596 45, 2789-2794, <https://doi.org/10.1016/j.atmosenv.2011.01.053>, 2011.
- 597 Peng, Z., Lei, L. L., Liu, Z. Q., Su, J. N., Ding, A. J., Ban, J. M., Chen, D., Kou, X. X., and Chu, K. K.: The impact of multi-species surface
598 chemical observation assimilation on air quality forecasts in China, *Atmos. Chem. Phys.*, 18, 18, [https://doi.org/10.5194/acp-18-17387-](https://doi.org/10.5194/acp-18-17387-2018)
599 2018, 2018.
- 600 Price, C., Penner, J., and Prather, M.: NO_x from lightning .1. Global distribution based on lightning physics, *J. Geophys. Res.-Atmos.*, 102,
601 5929-5941, <https://doi.org/10.1029/96jd03504>, 1997.
- 602 Randerson, J. T., Van Der Werf, G. R., Giglio, L., Collatz, G. J., and Kasibhatla, P. S.: Global Fire Emissions Database, Version 4.1
603 (GFEDv4), 10.3334/ornlDaac/1293, 2017.
- 604 Sakov, P. and Oke, P. R.: A deterministic formulation of the ensemble Kalman filter: an alternative to ensemble square root filters, *Tellus*
605 *Ser. A-Dyn. Meteorol. Oceanol.*, 60, 361-371, <https://doi.org/10.1111/j.1600-0870.2007.00299.x>, 2008.
- 606 Shi, X. and Brasseur, G. P.: The Response in Air Quality to the Reduction of Chinese Economic Activities During the COVID-19 Outbreak,
607 *Geophys. Res. Lett.*, 47, e2020GL088070, <https://doi.org/10.1029/2020gl088070>, 2020.
- 608 Shi, Z., Song, C., Liu, B., Lu, G., Xu, J., Van Vu, T., Elliott, R. J. R., Li, W., Bloss, W. J., and Harrison, R. M.: Abrupt but smaller than
609 expected changes in surface air quality attributable to COVID-19 lockdowns, *Sci. Adv.*, 7, eabd6696,
610 <https://doi.org/10.1126/sciadv.abd6696>, 2021.
- 611 Sindelarova, K., Granier, C., Bouarar, I., Guenther, A., Tilmes, S., Stavrakou, T., Muller, J. F., Kuhn, U., Stefani, P., and Knorr, W.: Global
612 data set of biogenic VOC emissions calculated by the MEGAN model over the last 30 years, *Atmos. Chem. Phys.*, 14, 9317-9341,
613 <https://doi.org/10.5194/acp-14-9317-2014>, 2014.
- 614 Skamarock, W. C.: A description of the advanced research WRF version 3, Ncar Technical, 113, 7-25, 2008.
- 615 Streets, D. G., Bond, T. C., Carmichael, G. R., Fernandes, S. D., Fu, Q., He, D., Klimont, Z., Nelson, S. M., Tsai, N. Y., Wang, M. Q., Woo,
616 J. H., and Yarber, K. F.: An inventory of gaseous and primary aerosol emissions in Asia in the year 2000, *J. Geophys. Res.-Atmos.*, 108,
617 23, <https://doi.org/10.1029/2002JD003093>, 2003.
- 618 Sulaymon, I. D., Zhang, Y., Hopke, P. K., Hu, J., Zhang, Y., Li, L., Mei, X., Gong, K., Shi, Z., Zhao, B., and Zhao, F.: Persistent high
619 PM_{2.5} pollution driven by unfavorable meteorological conditions during the COVID-19 lockdown period in the Beijing-Tianjin-Hebei
620 region, China, *Environ. Res.*, 198, 111186, <https://doi.org/10.1016/j.envres.2021.111186>, 2021.
- 621 Tang, G., Zhu, X., Hu, B., Xin, J., Wang, L., Munkel, C., Mao, G., and Wang, Y.: Impact of emission controls on air quality in Beijing
622 during APEC 2014: lidar ceilometer observations, *Atmos. Chem. Phys.*, 15, 12667-12680, <https://doi.org/10.5194/acp-15-12667-2015>,
623 2015.
- 624 Tang, X., Zhu, J., Wang, Z. F., and Gbaguidi, A.: Improvement of ozone forecast over Beijing based on ensemble Kalman filter with
625 simultaneous adjustment of initial conditions and emissions, *Atmos. Chem. Phys.*, 11, 12901-12916, 10.5194/acp-11-12901-2011, 2011.
- 626 Tang, X., Zhu, J., Wang, Z. F., Wang, M., Gbaguidi, A., Li, J., Shao, M., Tang, G. Q., and Ji, D. S.: Inversion of CO emissions over Beijing
627 and its surrounding areas with ensemble Kalman filter, *Atmos. Environ.*, 81, 676-686, <https://doi.org/10.1016/j.atmosenv.2013.08.051>,
628 2013.
- 629 van der Werf, G. R., Randerson, J. T., Giglio, L., Collatz, G. J., Mu, M., Kasibhatla, P. S., Morton, D. C., DeFries, R. S., Jin, Y., and van
630 Leeuwen, T. T.: Global fire emissions and the contribution of deforestation, savanna, forest, agricultural, and peat fires (1997–2009),
631 *Atmos. Chem. Phys.*, 10, 11707-11735, <https://doi.org/10.5194/acp-10-11707-2010>, 2010.



- 632 Wang, P., Chen, K., Zhu, S., Wang, P., and Zhang, H.: Severe air pollution events not avoided by reduced anthropogenic activities during
633 COVID-19 outbreak, *Resour. Conserv. Recycl.*, 158, 104814, <https://doi.org/10.1016/j.resconrec.2020.104814>, 2020.
- 634 Wang, S., Gao, J., Zhang, Y., Zhang, J., Cha, F., Wang, T., Ren, C., and Wang, W.: Impact of emission control on regional air quality: An
635 observational study of air pollutants before, during and after the Beijing Olympic Games, *J. Environ. Sci.*, 26, 175-180,
636 [https://doi.org/10.1016/S1001-0742\(13\)60395-2](https://doi.org/10.1016/S1001-0742(13)60395-2), 2014.
- 637 Wang, Z., Uno, I., Yumimoto, K., Itahashi, S., Chen, X., Yang, W., and Wang, Z.: Impacts of COVID-19 lockdown, Spring Festival and
638 meteorology on the NO₂ variations in early 2020 over China based on in-situ observations, satellite retrievals and model simulations,
639 *Atmos. Environ.*, 244, 117972, <https://doi.org/10.1016/j.atmosenv.2020.117972>, 2021.
- 640 Wu, H., Tang, X., Wang, Z., Wu, L., Li, J., Wang, W., Yang, W., and Zhu, J.: High-spatiotemporal-resolution inverse estimation of CO and
641 NO_x emission reductions during emission control periods with a modified ensemble Kalman filter, *Atmos. Environ.*, 236, 117631,
642 <https://doi.org/10.1016/j.atmosenv.2020.117631>, 2020.
- 643 Wu, H. J., Tang, X., Wang, Z. F., Wu, L., Lu, M. M., Wei, L. F., and Zhu, J.: Probabilistic Automatic Outlier Detection for Surface Air
644 Quality Measurements from the China National Environmental Monitoring Network, *Adv. Atmos. Sci.*, 35, 1522-1532,
645 <https://doi.org/10.1007/s00376-018-8067-9>, 2018.
- 646 Xing, J., Li, S. W., Jiang, Y. Q., Wang, S. X., Ding, D., Dong, Z. X., Zhu, Y., and Hao, J. M.: Quantifying the emission changes and
647 associated air quality impacts during the COVID-19 pandemic on the North China Plain: a response modeling study, *Atmos. Chem.
648 Phys.*, 20, 14347-14359, <https://doi.org/10.5194/acp-20-14347-2020>, 2020.
- 649 Yan, C., Shen, Y. C., Stolzenburg, D., Dada, L., Qi, X. M., Hakala, S., Sundstrom, A. M., Guo, Y. S., Lipponen, A., Kokkonen, T. V.,
650 Kontkanen, J., Cai, R. L., Cai, J., Chan, T., Chen, L. D., Chu, B. W., Deng, C. J., Du, W., Fan, X. L., He, X. C., Kangasluoma, J.,
651 Kujansuu, J., Kurppa, M., Li, C., Li, Y. R., Lin, Z. H., Liu, Y. L., Liu, Y. L., Lu, Y. Q., Nie, W., Pulliainen, J., Qiao, X. H., Wang, Y. H.,
652 Wen, Y. F., Wu, Y., Yang, G., Yao, L., Yin, R. J., Zhang, G., Zhang, S. J., Zheng, F. X., Zhou, Y., Arola, A., Tamminen, J., Paasonen,
653 P., Sun, Y. L., Wang, L., Donahue, N. M., Liu, Y. C., Bianchi, F., Daellenbach, K. R., Worsnop, D. R., Kerminen, V. M., Petaja, T.,
654 Ding, A. J., Jiang, J. K., and Kulmala, M.: The effect of COVID-19 restrictions on atmospheric new particle formation in Beijing, *Atmos.
655 Chem. Phys.*, 22, 12207-12220, <https://doi.org/10.5194/acp-22-12207-2022>, 2022.
- 656 Yan, X. Y., Akimoto, H., and Ohara, T.: Estimation of nitrous oxide, nitric oxide and ammonia emissions from croplands in East, Southeast
657 and South Asia, *Glob. Change Biol.*, 9, 1080-1096, <https://doi.org/10.1046/j.1365-2486.2003.00649.x>, 2003.
- 658 Zhang, L., Shao, J., Lu, X., Zhao, Y., Hu, Y., Henze, D. K., Liao, H., Gong, S., and Zhang, Q.: Sources and Processes Affecting Fine
659 Particulate Matter Pollution over North China: An Adjoint Analysis of the Beijing APEC Period, *Environ. Sci. Technol.*, 50, 8731-8740,
660 <https://doi.org/10.1021/acs.est.6b03010>, 2016.
- 661 Zhang, Q., Pan, Y., He, Y., Walters, W. W., Ni, Q., Liu, X., Xu, G., Shao, J., and Jiang, C.: Substantial nitrogen oxides emission reduction
662 from China due to COVID-19 and its impact on surface ozone and aerosol pollution, *Sci. Total Environ.*, 753, 142238,
663 <https://doi.org/10.1016/j.scitotenv.2020.142238>, 2021.
- 664 Zhang, R. X., Zhang, Y. Z., Lin, H. P., Feng, X., Fu, T. M., and Wang, Y. H.: NO_x Emission Reduction and Recovery during COVID-19 in
665 East China, *Atmosphere*, 11, 15, <https://doi.org/10.3390/atmos11040433>, 2020.
- 666 Zhang, W., Guo, J. H., Sun, Y. L., Yuan, H., Zhuang, G. S., Zhuang, Y. H., and Hao, Z. P.: Source apportionment for urban PM₁₀ and
667 PM_{2.5} in the Beijing area, *Chin. Sci. Bull.*, 52, 608-615, <https://doi.org/10.1007/s11434-007-0076-5>, 2007.
- 668 Zhao, X., Wang, G., Wang, S., Zhao, N., Zhang, M., and Yue, W.: Impacts of COVID-19 on air quality in mid-eastern China: An insight
669 into meteorology and emissions, *Atmos. Environ.*, 266, 118750, <https://doi.org/10.1016/j.atmosenv.2021.118750>, 2021.



- 670 Zhao, Y. B., Zhang, K., Xu, X. T., Shen, H. Z., Zhu, X., Zhang, Y. X., Hu, Y. T., and Shen, G. F.: Substantial Changes in Nitrogen Dioxide
671 and Ozone after Excluding Meteorological Impacts during the COVID-19 Outbreak in Mainland China, *Environ. Sci. Technol. Lett.*, 7,
672 402-408, <https://doi.org/10.1021/acs.estlett.0c00304>, 2020.
- 673 Zheng, B., Zhang, Q., Geng, G., Chen, C., Shi, Q., Cui, M., Lei, Y., and He, K.: Changes in China's anthropogenic emissions and air quality
674 during the COVID-19 pandemic in 2020, *Earth Syst. Sci. Data*, 13, 2895-2907, <https://doi.org/10.5194/essd-13-2895-2021>, 2021.
- 675 Zheng, B., Tong, D., Li, M., Liu, F., Hong, C. P., Geng, G. N., Li, H. Y., Li, X., Peng, L. Q., Qi, J., Yan, L., Zhang, Y. X., Zhao, H. Y.,
676 Zheng, Y. X., He, K. B., and Zhang, Q.: Trends in China's anthropogenic emissions since 2010 as the consequence of clean air actions,
677 *Atmos. Chem. Phys.*, 18, 14095-14111, <https://doi.org/10.5194/acp-18-14095-2018>, 2018.
- 678
- 679